Jour. Indian Association of Sedimentologists, Vol. 36, No. 2 (2019), pp.1-37
ISSN Online 2582 – 2020
ISSN Print 0970 – 3268

Global significance of wind forcing on deflecting sediment plumes at river mouths: Implications for hyperpycnal flows, sediment transport, and provenance

G. Shanmugam
Department of Earth and Environmental Sciences, The University of Texas at Arlington
Arlington, TX 76019, USA
Email: shanshanmugam@aol.com

Abstract: This review, based on sediment plumes at the mouths of 29 rivers worldwide, has revealed that sediment (density) plumes are commonly deflected away from the normal downslope direction in 18 out of 29 cases. These deflected sediment plumes have been documented at the mouths of Brisbane, Congo, Connecticut, Dart, Ebro, Eel, Elwha, Fonissa, Guadalquivir, Krishna-Godavari, Mississippi, Monros, Rio de la Plata, Pearl, Rhone, Tiber, Yellow, and Yangtze rivers. As a consequence, current directions change drastically and sediment distribution occurs on only one side of river mouths. In these cases, sediment transport is diverted by a plethora of 22 oceanographic, meteorological, and other external factors. Empirical data show that wind forcing is the most dominant factor. Other influencing factors are tidal currents, ocean currents, and coastal upwelling. Deflection of sediment plumes defies the conventional use of paleocurrent directions in determining sediment transport and provenance in the ancient sedimentary record. Failure to recognize deflected sediment plumes in the rock record could result in construction of erroneous depositional models with economic implications for reservoir prediction in petroleum exploration.

Keywords: Deflecting sediment plume, Elwha River**,** Hyperpycnal flows, Paleocurrents, Sediment transport, Tropical cyclone, Wind forcing

Introduction

Density plumes and their various configurations seen on satellite images have been a source of curiosity to the geologic community as well as to the general public. The U.S. National Aeronautics and Space Administration (NASA, 2019) has archived satellite images on density plumes in its online publishing outlet "Earth Observatory" since 1999. NASA has used a variety of satellites, such as Aqua, Terra and Topex/Poseidon. However, there has not been a systematic attempt to compile

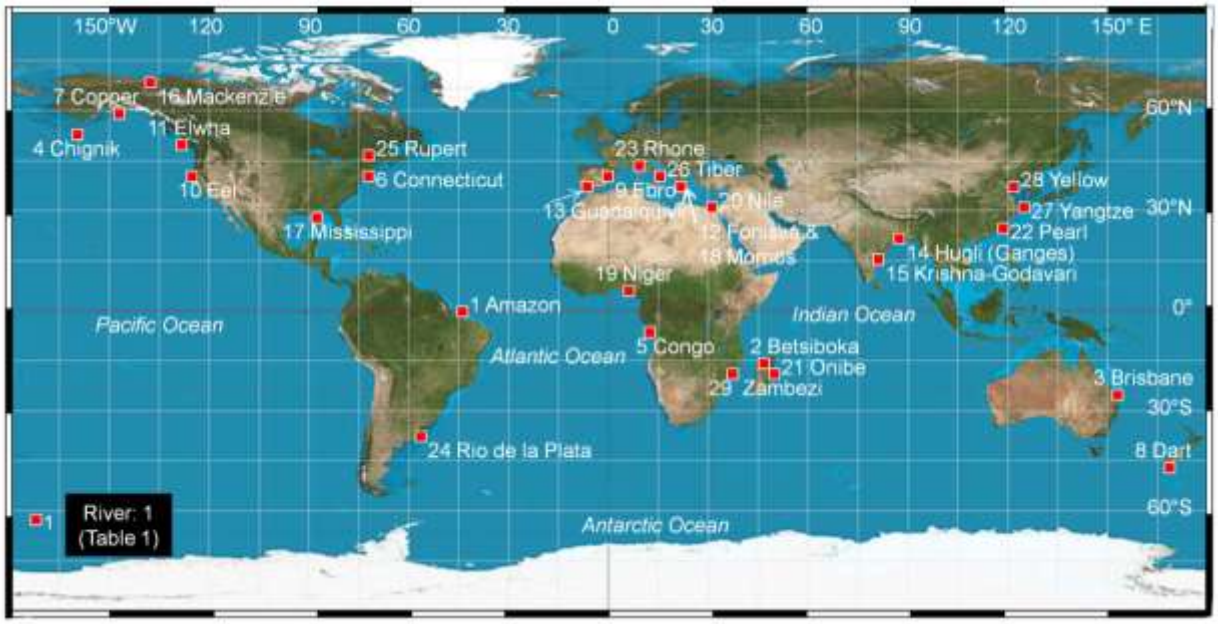

Fig. 1. Location map of 29 rivers used in this study. See Table 1 for details.

variations in natural configurations of density plumes in the world's oceans and lakes (Shanmugam, 2018a, b). This article is an attempt to report common occurrence of density plumes that are deflected at river mouths worldwide due to various external controlling factors (Fig. 1, Table 1).

Serial Number (Fig. 1)	Case study and Location	Coalescing	Environment	External control	Comments
1	Amazon River, Brazil, Equatorial Atlantic	Deflecting	Open marine	Ocean currents and phytoplankton	Natural sediment plume
2	Betsiboka River, NW Madagascar	Massive	Bay	Tides	Natural sediment plume
3	Brisbane River, Australia, Moreton Bay	Deflecting (Fig. 17)	Bay	Tides	Anthropogenic, due to Port of Brisbane
4	Chignik River, Alaska, Pacific Ocean	Linear	Braid delta in a lagoon, Pacific Ocean	Coarse-grained braid delta (McPherson et al., 1987)	Natural sediment plume
5	Congo (Zaire) River, W. Africa	Deflecting (Fig. 12)	Marine	Tidal currents (Shanmugam, 2003)	Natural sediment plume
6	Connecticut River, New England region, USA	Deflecting (Fig. 5A)	Long Island Sound	Wind forcing (Hurricane Irene, August 21-30, 2011)	Natural sediment plume
7	Copper River, USA, Gulf of Alaska	Coalescing	Braid delta, Marine	Eolian	Natural sediment plume

8	Dart River, South Island, New Zealand, Lake Wakatipu	Deflecting (Fig. 18C)	Braid delta, lacustrine	Tidal? (Heath, 1975)	Natural sediment plume
9	Ebro Delta, Iberian Peninsula, Mediterranean Sea	Deflecting (Fig. 8B)	River-dominated delta	Wind forcing, Cyclonic events and Ocean currents (Arnau et al., 2004)	Natural sediment plume
10	Eel River, California, USA	Deflecting (Fig. 5B)	Shelf	Wind forcing and Shelf currents (Geyer et al., 2000; Imran and Syvitski, 2000)	Natural sediment plume
11	Elwha River, Washington, USA, Strait of Juan de Fuca	Deflecting (Fig. 3C)	Strait	Tidal currents (Cannon, 1978; Thomson et al., 2007), and upwelling wind currents (Foreman et al., 2008)	Anthropogenic plume caused by dam demolition
12	Fonissa River, Greece, Gulf of Corinth	Deflecting (Fig. 11C)	Delta	Bottom currents (Beckers et al., 2016)	Natural sediment plume
13	Guadalquivir River, Southern Spain, Gulf of Cádiz	U-Turn (Deflecting) (Fig. 9C)	River-dominated delta	Surface and slope currents (Peliz et al., 2009)	Natural sediment plume
14	Hugli River, a tributary of the Ganges River, India, Bay of Bengal	Anastomosing	Tide-dominated estuary (Balasubramanian and Ajmal Khan, 2002)	Tidal currents	Natural sediment plume
15	Krishna-Godavari Rivers, India, Bay of Bengal	Deflecting (Fig. 15 & 16)	Estuary	Tidal currents (Shanmugam et al., 2009)' Monsoonal currents (Jagadeesan et al., 2013), and geostrophic currents (Sridhar et al., 2008)	Natural sediment plume
16	Mackenzie River Delta, Canada, Beaufort Sea	Swirly	River-dominated delta	Arctic ocean currents	Natural sediment plume
17	Mississippi River, USA, Gulf of Mexico	Deflating (Fig. 2D & 6B)	River-dominated delta	Wind forcing, **shelf currents** (Walker and Rouse, 1993)	Natural sediment plume
18	Mornos River, Greece, Gulf of Corinth	Deflecting (Fig. 11B)	Delta	Bottom currents (Beckers et al., 2016)	Natural sediment plume
19	Niger River, W. Arica	Linear	Wave-dominated delta	Wind forcing, wave currents	Natural sediment plume
20	Nile Delta, Egypt, Mediterranean Sea	Lobate	River-dominated delta	Wind forcing	Natural sediment plume

21	Onibe River, Eastern Madagascar	Dissipating with sharp front	Marine	Wind forcing, Cyclone (Giovanna, February 7-24, 2012) and ocean currents	Natural sediment plume
22	Pearl River, henna, South China Sea	Deflecting (Fig. 14C)	Marine	Upwelling jets (Chen et al., 2017)	Natural sediment plume
23	Rhone Delta, France, Gulf of Lions, Mediterranean Sea	Deflecting (Fig. 8A)	River-dominated delta	Ocean currents (Arnau et al., 2004)	Natural sediment plume
24	Rio de la Plata Estuary, Argentina and Uruguay, South Atlantic Ocean	Dissipating and deflecting (Fig. 7C)	Marine	Ocean currents (Gonzalez-Silvera et al. 2006; Matano et al., 2010)	Natural sediment plume
25	Rupert Bay, Quebec	Swirly	Bay	Mixing of river and seawater combined with churn of tides	Natural sediment plume
26	Tiber River, Italy, Tyrrhenian Sea	Deflecting (Fig. 10B)	Marine	Wind forcing, Longshore currents (Mikhailova et al., 1998).	Natural sediment plume
27	Yangtze River; China, East China Sea	Deflecting (Fig. 13A)	Tide-dominated estuary	Shelf currents (Liu et al., 2006), Vertical mixing by tides in winter months (Luo et al., 2017)	Natural sediment plume
28	Yellow River, China, Bohai Bay	Horse's tail (Deflecting) (Fig. 2E), Lobate (Fig. 2F)	River-dominated delta	Tidal shear front (Wang et al., 2010)	Natural sediment plume
29	Zambezi River, Central Mozambique, India Ocean	Coalescing lobate, associated with multiple river mouths	Wave-dominated delta	Wind forcing, Longshore currents (Mikhailov et al., 2015)	Natural sediment plume

Table 1. Case studies of 29 rivers, their sediment plumes, and external controls.

Bates (1953) suggested three types of density plumes at river-mouth deltaic environments: 1) hypopycnal plume for floating river water that has lower density than basin water (Fig. 2A); 2) homopycnal plume for mixing river water that has equal density as basin water (Fig. 2B); and 3) hyperpycnal plume for sinking river water that has higher density than basin water (Fig. 2C). Although river-mouth hyperpycnal plumes have received much attention (Bates, 1953), plumes in other environments (e.g., lakes) are equally important.

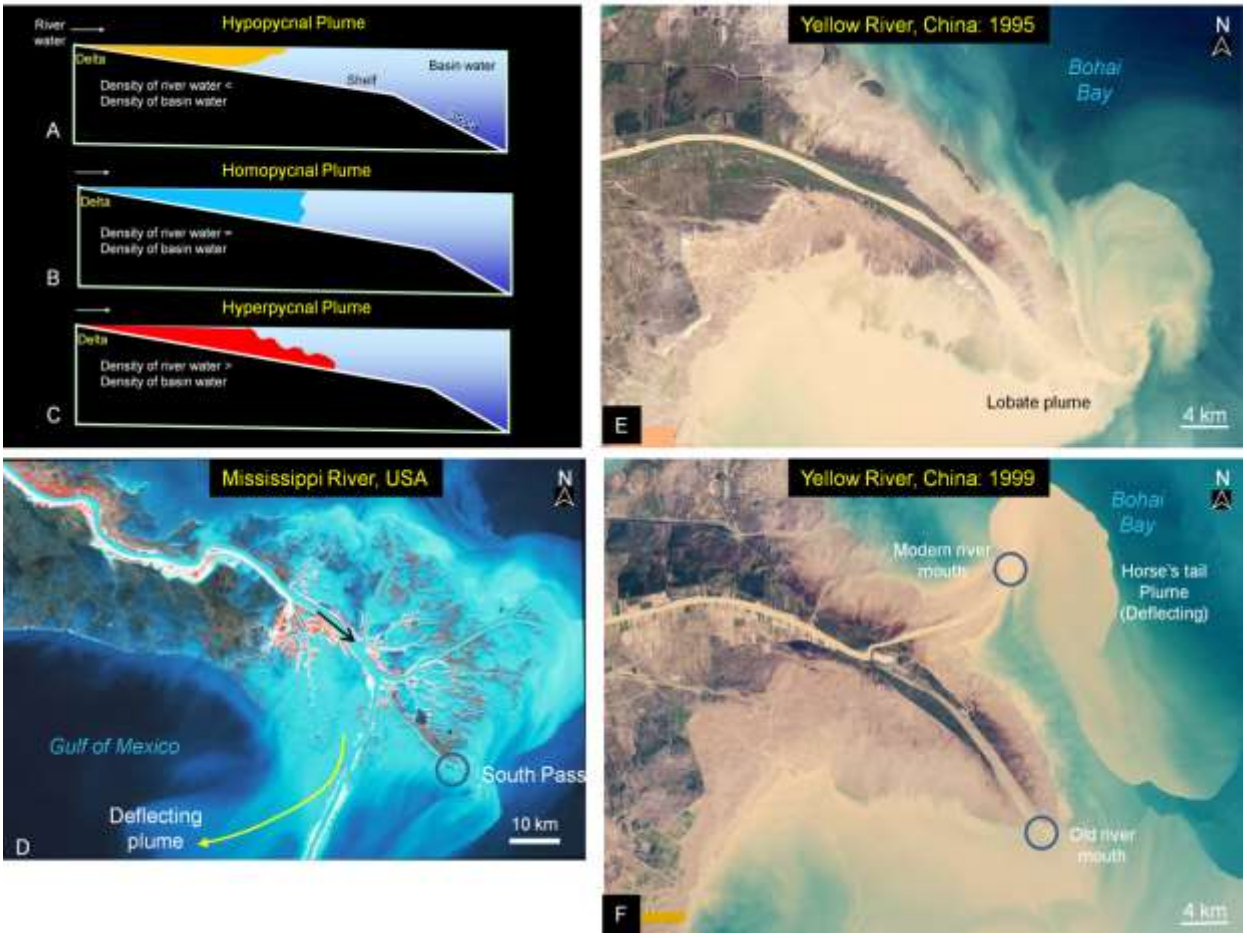

Fig. 2. A. B. C. Schematic diagrams showing three types of density plumes at river mouths in deltaic environments based on concepts of Bates (1953). Figure from Shanmugam (2012) with permission from Elsevier. D. Image of the Mississippi River showing well-developed deflecting plume (yellow arrow). Circle shows river mouth. E. Satellite image of the Yellow River showing well-developed lobate plume at the old river mouth. F. Satellite image of the Yellow River showing horse's tail (deflecting) plume at the modern river mouth that was initiated in 1996. Two circles show old and modern river mouths. From Shanmugam (2018a).

River mouths constitute an important intersectional setting between terrestrial and marine or lacustrine environments. In terms of processes that influence river-mouth sedimentation are waves (Komar, 1976), tides (Klein (1970), gravity-driven downslope processes (Middleton and Hampton, 1973), cyclones (Shanmugam, 2008), tsunamis (Shanmugam, 2008), and shelf-edge related currents (Southard and Stanley, 1976). In addition to longshore currents (Komar, 1976), there are cross-shelf currents (Brink, 2016) and upwelling currents (Milliff et al. 2004; Foreman et al., 2008) that affect the river-mouth and shelf environments.

The primary purpose of this is to document the common occurrence of deflected sediment plumes at river mouths. The second objective is to document the types of external controls involved in deflecting sediment plumes. The third objective is to discuss implications of sediment deflections in understanding paleocurrents, paleogeography, provenance, and reservoir distribution in the ancient sedimentary record. Although the primary dataset for this study is from NASA's satellite images, other published photographic and other images are also used.

Dataset

The term 'sediment plume' is used here for plumes in which the primary cause of density is sediment, although salinity and temperature are important in some cases. A plume is defined a fluid enriched in sediment, ash, biological or chemical matter that enters another fluid. NOAA Fisheries Glossary (2006, p. 42) defines a *River Plume* as "*Turbid freshwater flowing from land and generally in the distal part of a river (mouth) outside the bounds of an estuary or river channel*." Because the original concept of hyperpycnal flows is closely tied to river floods, density plumes at river mouths are considered using the following 29 rivers in this study (Fig. 1):

1) Amazon River, Equatorial Atlantic, Brazil.
2) Betsiboka River, Bombetoka Bay, NW Madagascar.
3) Brisbane River, Moreton Bay, Australia.
4) Chignik River, Alaska, Pacific Ocean, USA.
5) Congo (Zaire) River, South Atlantic Ocean, West Africa.
6) Connecticut River, New England region, USA, Long Island Sound, USA.
7) Copper River, Gulf of Alaska, USA.
8) Dart River, South Island, Lake Wakatipu, New Zealand.
9) Ebro River, Mediterranean Sea, Iberian Peninsula.
10) Eel River, California, Pacific Ocean, USA.
11) Elwha River, Strait of Juan de Fuca, USA.
12) Fonissa River, Gulf of Corinth, Greece.
13) Guadalquivir River, Gulf of Cádiz, Southern Spain.
14) Hugli River (a distributary of the Ganges River), Bay of Bengal, India.

15) Krishna-Godavari Rivers, Bay of Bengal, India.
16) Mackenzie River, Beaufort Sea, Canada.
17) Mississippi River, Gulf of Mexico, USA.
18) Mornos River, Gulf of Corinth, Greece.
19) Niger River, North Atlantic Ocean, West Africa.
20) Nile River Delta, Mediterranean Sea, Egypt.
21) Onibe River, Indian Ocean, Eastern Madagascar.
22) Pearl River, South China Sea, China.
23) Rhone River, Gulf of Lions, Mediterranean Sea, France.
24) Rio de la Plata Estuary, South Atlantic Ocean, Argentina and Uruguay.
25) Rupert River, Quebec, Rupert Bay, Canada.
26) Tiber River, Tyrrhenian Sea, Italy.
27) Yangtze River, East China Sea, China.
28) Yellow River, Bohai Bay, Bohai Sea, China.
29) Zambezi River, Indian Ocean, Central Mozambique.

External control of deflected sediment plumes

External controls are allogenic in nature, which are external to the depositional system, such as uplift, subsidence, climate, eustacy, etc. However, external controls of density plumes are much more variable and include some common depositional processes (e.g., tidal currents, wind forcing, cyclones, etc.). In addition, local physiographic elements, such as seafloor-ridges, channels, etc. could influence the path of plumes. Anthropogenic structures are also known to control deflection of plumes. In this study, the deflection of sediment transport away from the normal downslope transport, by mechanisms, such as longshore currents, is emphasized.

Elwha sediment plume, Strait of Juan de Fuca

The Elwha River is 72 km long in the Olympic Peninsula in the U.S. state of Washington. From its source at Elwha snowfinger in the Olympic Mountains, it flows generally north to the Strait of Juan de Fuca at the U.S.- Canada border (Fig. 3A). A spectacular example of an anthropogenic Elwha sediment plume was triggered by the demolition of Elwha Dam in the Olympic Peninsula, State of Washington (Fig. 3AB). This sediment plume (Fig. 3C)

Fig. 3. Sediment plume triggered by Elwha Dam demolition in the State of Washington (USA). A. Index map showing Elwha Dam (arrow). The 108-foot dam, built in 1910 and demolished in 2012, is located approximately 7.9 km upstream from the river mouth. Credit: U.S. Geological Survey Public Domain map. B. Aerial photograph of the Olympic Peninsula and the Strait of Juan de Fuca. Filled yellow circle = Elwha River mouth. From Duda et al. (2011) with additional labels by G. Shanmugam. C. Elwha sediment plume triggered by the demolition of Elwha Dam in 2012. Red arrow shows easterly deflecting plume, away from the Pacific Ocean. This deflection could be attributed to tidal currents in this estuarine environment. Also, the Strait of Juan de Fuca is subjected to easterly upwelling winds (see Fig. 4). Photo credit: Tom Roorda. Aerial photo was taken on March 30, 2012. D. Aerial photo of Elwha River mouth showing absence of sediment plume in 2019 (compare with Fig. 3C). Aerial photo was taken on February 28, 2019. Photo courtesy of Tom Roorda, Roorda Aerial, Port Angeles, WA.

was the result of sediment released from the world's largest dam demolition (Ritchie et al., 2018). The University of Washington (Seattle, WA) first reported this phenomenal event and its oceanographic and sedimentologic implications in the UW News (Hickey, 2013). According to USGS (2018), this demolition event flushed out 20 million tons of sediment into the Strait of Juan de Fuca. One could classify these Elwha sediment plumes (Fig. 3C) as modern hyperpycnal flows based on visual

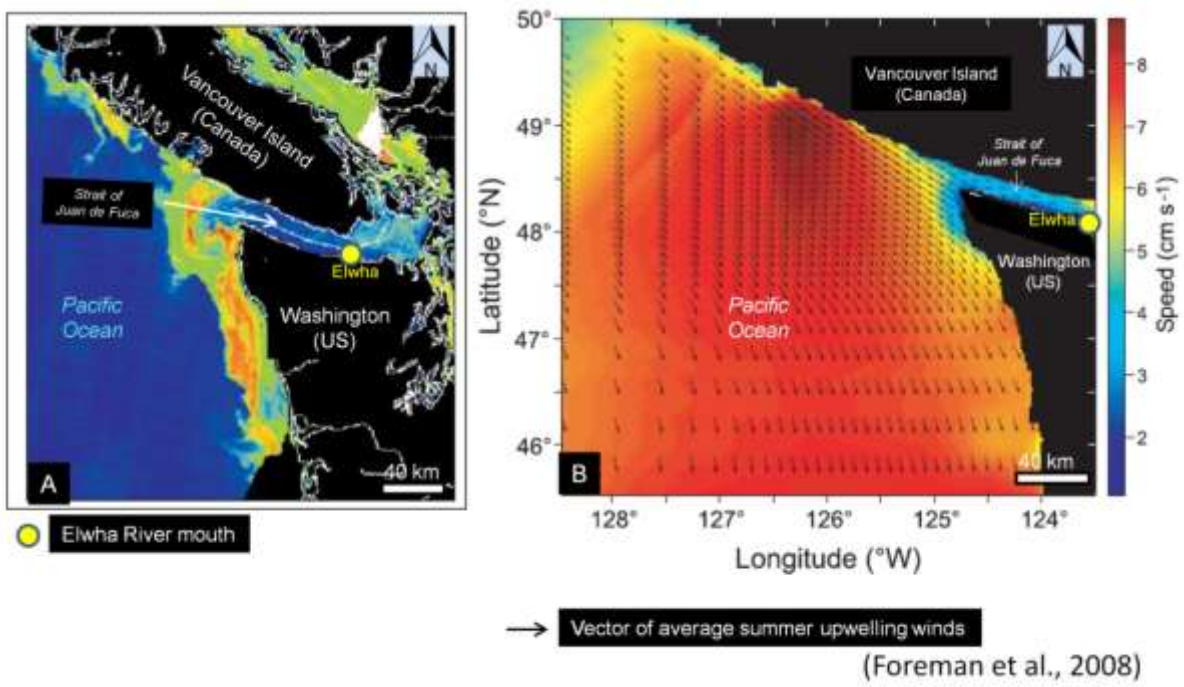

Fig. 4. External control of sediment plumes in the Strait of Juan de Fuca. A. MERIS (MEdium Resolution Imaging Spectrometer) satellite image showing oceanographic setting of the Strait of Juan de Fuca. Filled yellow circle = Elwha River mouth. Satellite image courtesy of the European Space Agency. B. Average summer Upwelling winds, which move easterly in the strait could explain deflecting plumes observed at the Elwha River mouth (see Fig. 3C). According to Foreman et al. (2008), winds reach a maximum speed of 8 m s^{-1} off Vancouver Island with increasing magnitudes eastward in the Strait of Juan de Fuca. Filled yellow circle = Elwha River mouth. Both images are from Foreman et al. (2008) with additional labels by G. Shanmugam.

observation alone. However, without measurements of fluid theology, flow state, and flow density, any classification of these Elwha plumes either as hyperpycnal flows, or as turbidity currents, or as sandy debris flows, is problematic.

Despite the uncertain nature of flow types, an important lesson learned from the Elwha sediment plume is that external factors are critical in redirecting sediment transport. The deflection of Elwha plume to the east (Fig. 3C) could be attributed to tidal currents in this estuarine environment (Cannon, 1978; Thomson et al., 2007; Warrick et al., 2011). Also, summer upwelling winds move easterly into the Strait of Juan de Fuca Fig. 4B). Such summer winds could also explain deflecting sediment plume to the east of the Elwha River mouth (Fig. 3C). The reason is that winds reach a maximum speed of 8 m s^{-1} off Vancouver Island with increasing magnitudes eastward in the Strait of Juan de Fuca (Foreman et al., 2008).

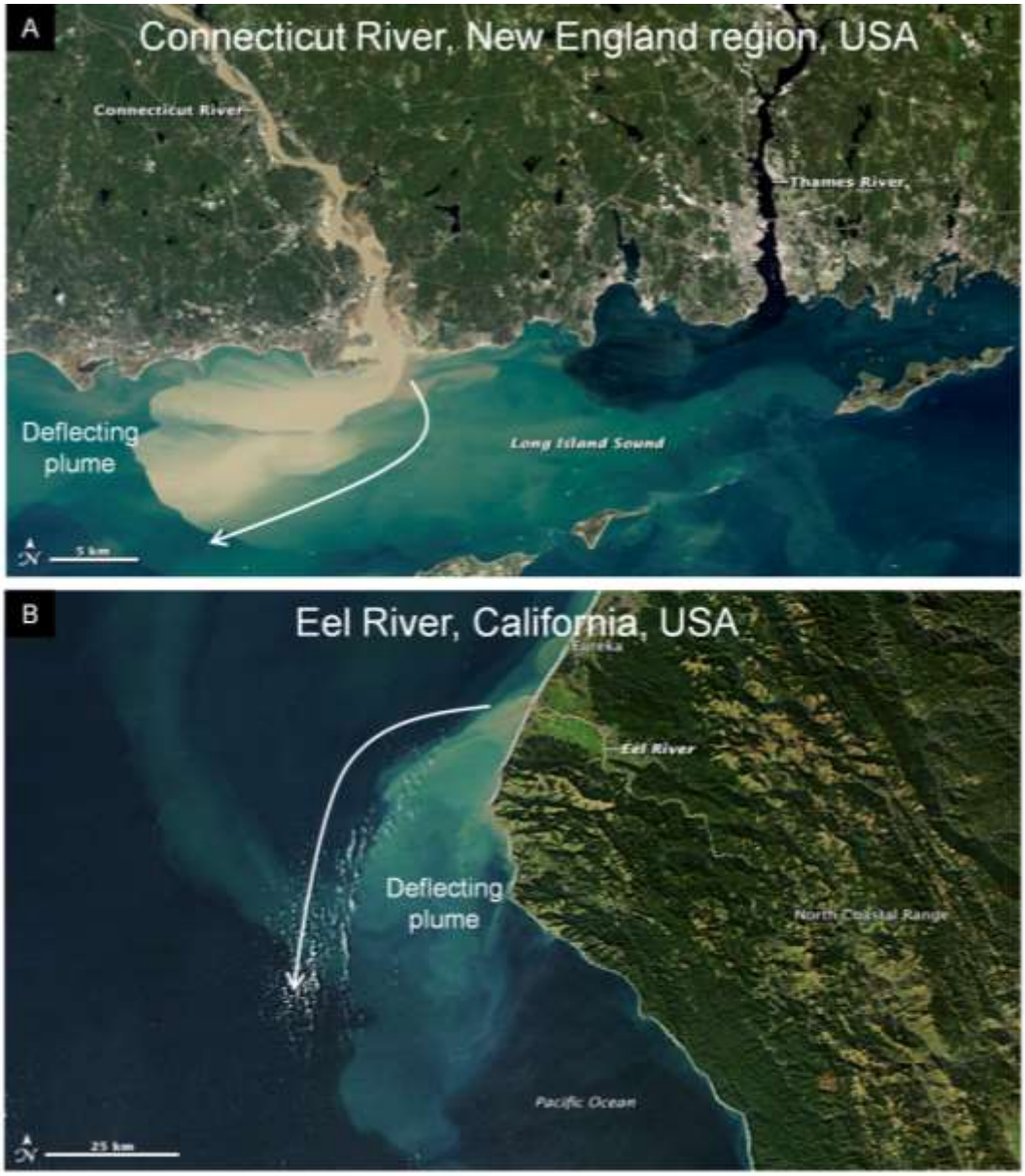

Fig. 5. A. Satellite image showing the Connecticut River entering the Long Island Sound with a deflected lobate plume. NASA Earth Observatory image by Robert Simmon. Image acquired on September 2, 2011. B. Satellite image showing the Eel River in California with a deflected lobate plume. NASA image courtesy Jeff Schmaltz, LANCE MODIS Rapid Response. Caption by Adam Voiland. Image acquired on December 9, 2012.

Connecticut River, New England region, USA, Long Island Sound

The Connecticut River is the longest river in the New England region of the United States. It flows roughly southward for 653 km through four states. It originates at the U.S. border with Quebec, Canada, and empties into Long Island Sound. After Hurricane Irene drenched New England with rainfall in late August 21-30,

2011, the Connecticut River was spewing muddy sediment into Long Island Sound.

Satellite image showed the Connecticut River entering the Long Island Sound deflected lobate plumes (Fig. 5A). The image was acquired on September 2, 2011, two days after the storm dissipated. However, the storm became extratropical cyclone on August 28 and lingered on for a few days. Therefore, the cause of plume deflection could still be the post-hurricane winds associated with the extratropical cyclone.

Eel River, California, USA, Pacific Ocean

The Eel River about 315 km long in northern California where it empties into the Pacific Ocean. A satellite image of the Eel River shows a southerly deflection of sediment plume (Fig. 5B). Imran and Syvitski (2000) studied the Northern California Margin near the mouth of the Eel River and suggested that hyperpycnal flows may be influenced by the along-shelf currents and be deflected northward. Geyer et al. (2000) reported both southerly and northerly winds in the area, and thus the southerly deflection of plume shown in the NASA image (Fig. 5B) can be attributed to wind-forcing.

Mississippi River, USA, Gulf of Mexico

The Mississippi River is the second-largest drainage system on the North

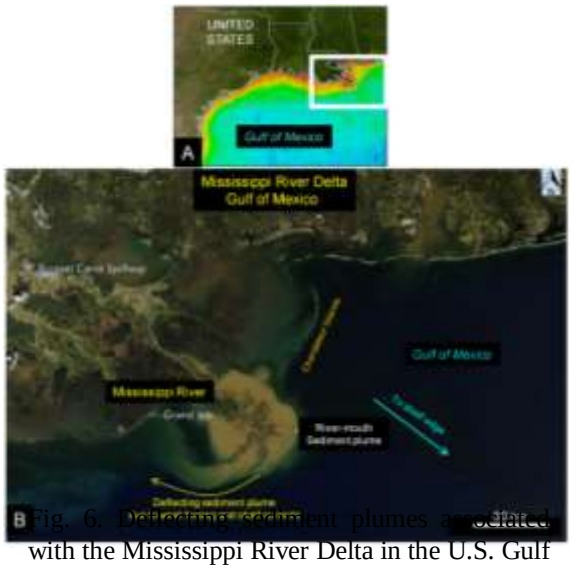

Fig. 6. Deflecting sediment plumes associated with the Mississippi River Delta in the U.S. Gulf of Mexico. A. Index map showing position of the Mississippi River Delta (Box). Image Credit: NASA. B. NASA satellite image of the Mississippi River (USA) showing deflecting (yellow arrow) sediment plumes (i.e., hyperpycnal plumes) away from the shelf edge due to external factors, such as wind forcing and shelf currents (Walker and Rouse, 1993). Image credit: *NASA Earth Observatory image by Joshua Stevens, using MODIS data from LANCE/EOSDIS Rapid Response*. Image acquired on March 4, 2018. Additional labels and interpretation by G. Shanmugam.

American continent, second only to the Hudson Bay drainage system. Its source is Lake Itasca in northern Minnesota and it flows generally south for 2,320 miles (3,730 km)[15] to the Mississippi River Delta in the Gulf of Mexico. A convincing example of deflecting sediment plume is revealed by the Mississippi River Delta in a

Fig. 7. A. Index map of the Río de la Plata Estuary. a Location of the Río de la Plata Estuary (white circle). Image credit: ETOPO1 Global Relief Model, C. Amante and B.W. Eakins, ETOPO1 Arc-Minute Global Relief Model: Procedures, Data Sources and Analysis, NOAA Technical Memorandum NESDIS NGDC-24, March 2009; B. Satellite image showing the Río de la Plata Estuary. C.Satellite image showing the Río de la Plata Estuary with hyperpycnal plumes that tend to deflect towards the Argentinian shelf to the south. Framiñan and Brown (1996) used the term "turbidity front" for this hyperpycnal plume. Note that the entire, 220-km wide, plume gets diluted and dissipated with an irregular front, which fails to advance into the South Atlantic. This dilution of plume is attributed to external controls, such as ocean currents operating on the shelf. The Paraná River, the second longest river in South America after the Amazon, supplies three-quarters of the fresh water that enters the estuary, with the remainder arriving from the Uruguay River. See Fossati and Piedra-Cueva (2013). Figure from Shanmugam (2018a, b).

recent NASA satellite image (Fig. 6). These deflecting (Fig. 6B, yellow arrow) sediment plumes (i.e., hyperpycnal plumes) away from the shelf edge due to external factors, such as wind forcing and shelf currents (Walker et al., 1993) are clear evidence that hyperpycnal flows do not transport sediment across the shelf into deep-water environments.

Río de la Plata estuary, Argentina and Uruguay, South Atlantic Ocean

The Río de la Plata Estuary is located on the east coast of South America, bordering Argentina and Uruguay. It is 280 km long and

220 km wide at its mouth, and its water depth does not exceed 10 m (Fig. 7B). It receives water and sediment from both the Paraná and Uruguay rivers with an annual mean discharge of 22,000 m^3 s^{-1}. Satellite images show dissipating in the north and deflecting in the south plume with an irregular front (Fig. 7C).

The dissipating and deflecting functions of the plume can be attributed to ocean currents that are active at the mouth of the estuary in the South Atlantic ((Gonzalez-Silvera et al. 2006; Matano et al., 2010; Shanmugam, 2018a).

Rhone River, France, Gulf of Lions, Mediterranean Sea

The Rhone River is one of the major rivers of Europe. It originates in the Rhone Glacier in the Swiss Alps and empties into the Mediterranean Sea. In understanding river mouth plume-dispersion patterns in the Mediterranean Sea, Arnau et al. (2004) have utilized satellite imagery products, including various types of thermal and visible images (Advanced Very High Resolution Radiometer [AVHRR], Sea-viewing Wide Field-of-view Sensor [SeaWiFS], and Moderate Resolution Imaging Spectroradiometer [MODIS]). These images were used to describe plume-formation events, their association with coastal oceanography, and their dispersal in the northwestern Mediterranean Sea. At this location, two of the largest Mediterranean rivers (Rhone and Ebro) open into this virtually land-locked sea. Arnau et al. (2004) discussed whether flood events in the study area, as conditioned by riverine,

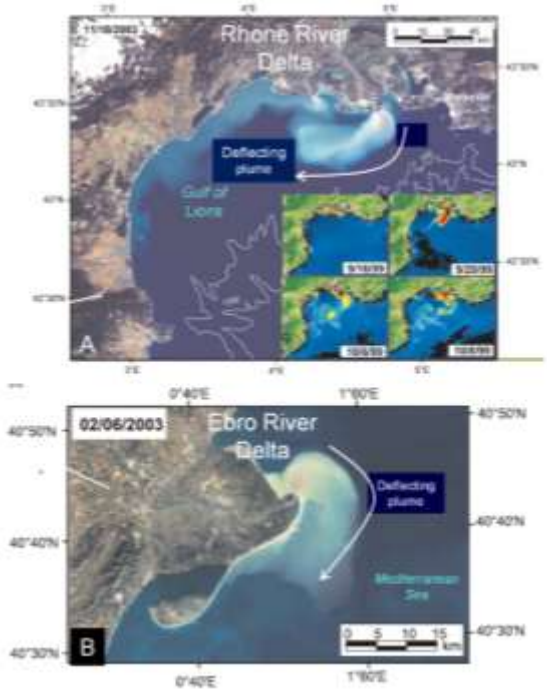

Fig. 8. Rivers flowing into the northern Mediterranean Sea. A. Satellite image showing deflected plume of the Rhone River. B. Satellite image showing deflected plume of the Ebro River. Both images from Arnau et al. (2004) with additional labels by G. Shanmuagm.

oceanographic, and climatic factors. In this study, we are concerned with the spectacular images of the Rhone River and its deflecting plume. (Fig. 8A). Ocean currents are

considered an important factor in deflecting these plumes.

Ebro Delta, Iberian Peninsula, Mediterranean Sea

The Ebro River is the second longest river in the Iberian peninsula after the Tagus. Arnau et al. (2004) discussed various aspects of Ebro River. A deflecting plume at the mouth of the Ebro River is striking (Fig. 8B). Cyclonic events and ocean currents are considered an important factor in deflecting these plumes.

Guadalquivir River, Southern Spain, Gulf of Cádiz

The Guadalquivir River is a major river the Iberian Peninsula with its entire length of 657 km in Spain . It empties into the Gulf of Cadiz to the south. The Gulf of Cádiz is located in the northeastern Atlantic Ocean (Fig. 9A). It is enclosed by the southern Iberian and northern Moroccan margins, west of the Gibraltar Strait. Two major rivers, the Guadalquivir and the Guadiana, as well as smaller rivers, like the Odiel, the Tinto, and the Guadalete, reach the ocean here. In terms of ocean currents (Peliz *et al*., 2009), it is one of the most complex oceanographic settings (Fig. 9B). Mimicking the current patterns, sediments that are emptied into the gulf by the Guadalquivir River exhibit a U-Turn

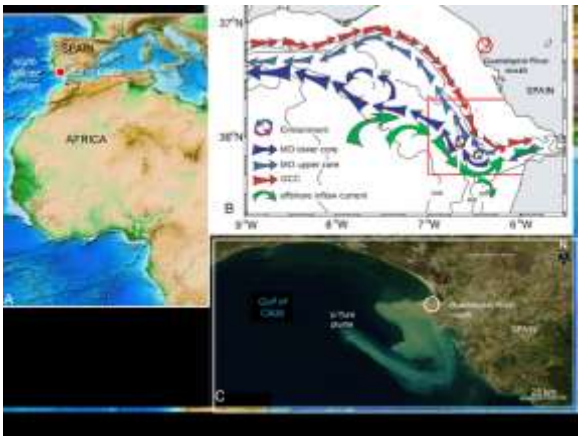

Fig. 9. A. Location map of the Gulf of Cádiz (red filled circle). B. Circulation patterns of ocean currents in the Gulf of Cádiz (Peliz et al. 2009). MO = Mediterranean outflow; GCC = Gulf of Cádiz slope current. C. Satellite image showing sediment plumes with an U-Turn pattern (white arrow). Note that the U-Turn pattern is mimicking the circulation of ocean currents (Fig. 9B). White open circle = Guadalquivir River mouth. NASA. Additional symbols and labels all by G. Shanmugam

shape for the plume (Fig. 9C). In cases like this, one must consider the influence of ocean currents on the dispersal of hyperpycnite sediments. The problem is that how these hyperpycnite sediments would differ from those hyperpycnites unaffected by ocean currents. In other words, do plume configurations (*i.e.*, U-Turn *versus* lobate) matter in the depositional record? No one has addressed this issue.

Tiber River, Italy, Tyrrhenian Sea

The Tiber River originates in the Apennine Mountains in Emilia-Romagna and flowing 406 kilometers (252 mi)through Tuscany, Umbria and Lazio

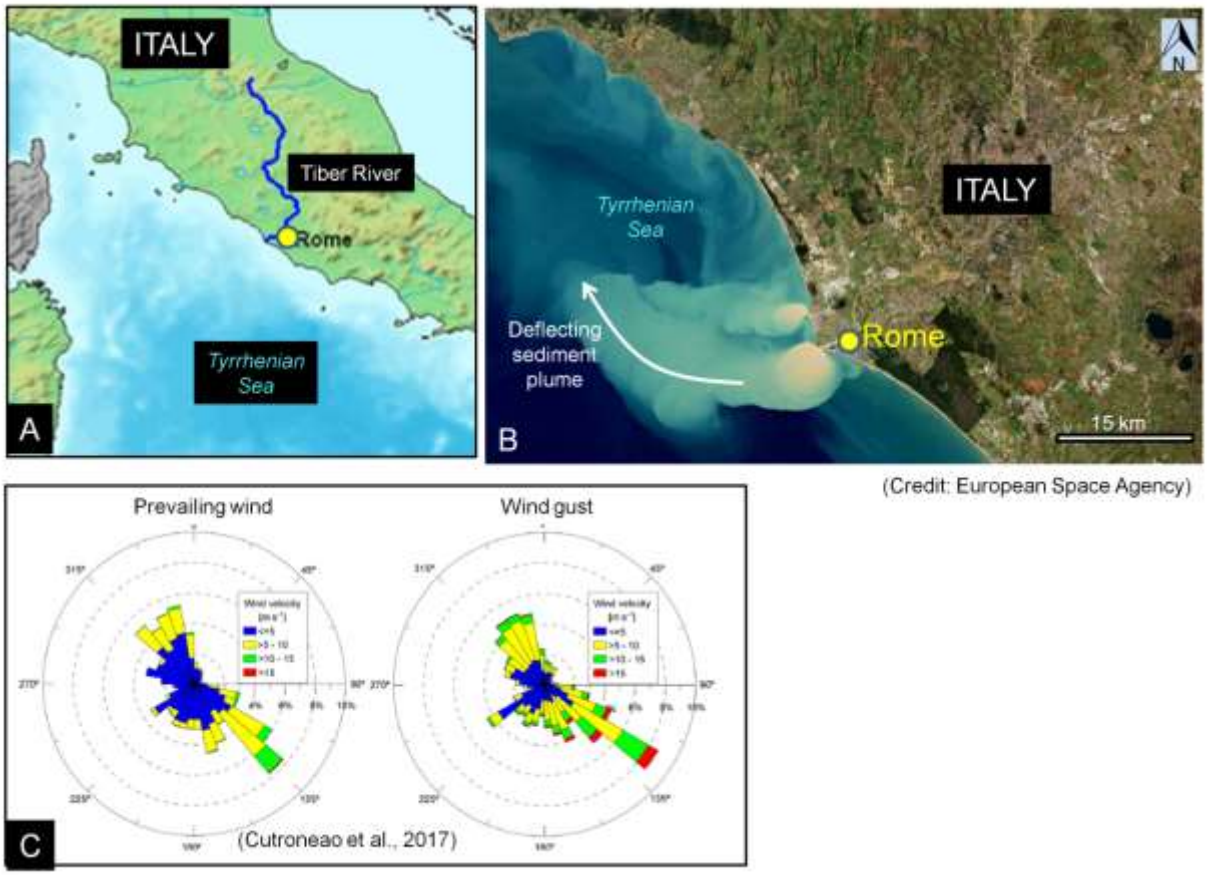

Fig. 10. Deflecting sediment plumes associated with the Tiber River, Tyrrhenian Sea. A. Index map of Tiber River Delta near Rome, Italy. Map modified after Wikipedia. B. The Copernicus Sentinel-2B satellite true-color image showing deflecting sediment plume at the mouth of the Tiber River. Note northwest trending plume (arrow) controlled by northwesterly wind (Manca et al., 2014) and by northwesterly flowing longshore currents at the river mouth (Mikhailova et al., 1998). Credit: Copernicus Sentinel data (2019), processed by ESA, CC BY-SA 3.0 IGO. Image captured on February 5, 2019. C. Rose diagrams showing the velocity and the direction of prevailing wind (left panel) and the maximum velocity and direction of gusts (right panel) in the Giglio Island, which is located northwest of the Tiber delta. Measurements were made every 10 minutes at the weather station of Giglio Porto during the study period 2012-2013. Giglio Porto is located 185 km northwest of Rome. Note that wind is trending from SSE to NNW direction (compare with northwest-trending plume direction in Fig. 10B). From Cutroneao et al. (2017) with permission from Elsevier.

, and empties into the Tyrrhenian Sea, near Rome. A satellite image of sediment plumes associated with the Tiber River in Italy also shows deflected plumes due to northwesterly wind and longshore currents along the Tyrrhenian coast (Fig. 10). The northwest-trending plume (arrow in Fig. 10B) controlled by northwesterly wind (Manca et al., 2014) and by northwesterly flowing longshore currents at the river mouth (Mikhailova et al., 1998). This is a wave-dominated delta (Milli et al., 2013).

Monros and Fonissa Rivers, Greece, Gulf of Corinth

from0.4 to 2.2 m long were retrieved in 2011 and 2014 with UWITEC® and BENTOS®

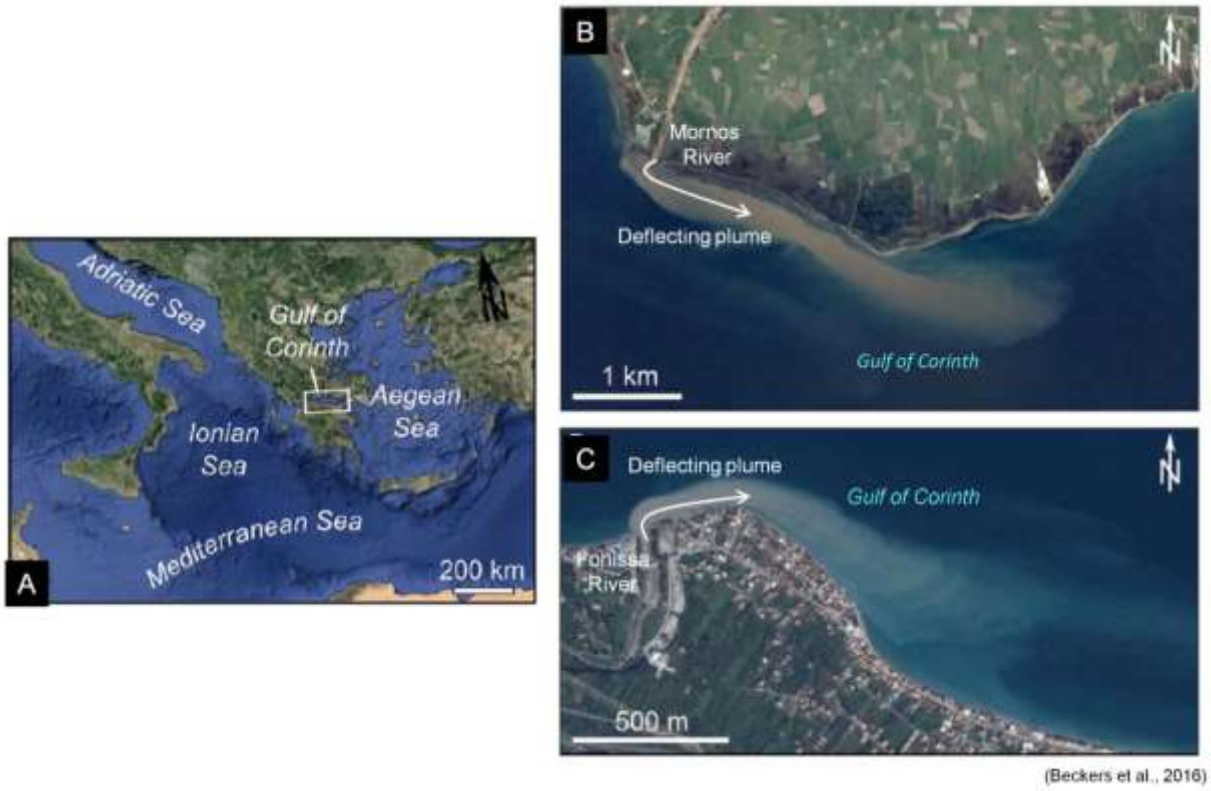

Fig. 11. A. Index map showing Gulf of Corinth, Greece. B. Deflected plume associated with Mornos River. C. (Deflected plume associated with Fonissa River. From Beckers et al. (2016) with additional labels by G. Shanmugam.

The Gulf of Corinth is a 120 km long, up to 30 km wide, and 867 m deep water body connected to the Ionian Sea, in Greece (Fig. 11A). The Gulf is connected at its western tip to the Mediterranean Sea through three shallow sills. Beckers et al. (2016) discussed the influence of bottom currents on deflecting sediment plumes in two rivers, namely the south-flowing Monros River (Fig. 11B) and the north-flowing Fonissa River (Fig. 11C) into the Gulf of Corinth. Twelve cores gravity corers. The cores are located at various depths and various distances from the Rion straits. These cores indicate that drifts are composed of homogenous bioturbated mud in their upper part. This core study is one of the rare cases in which the authors attempt to relate deflection of sediment plumes at river mouths to bottom currents and to link the shallow-water drift deposit to bottom currents. Types of bottom currents, including

contour currents, are discussed by Shanmugam (2016).

Congo (Zaire) River, West Africa, Atlantic Ocean

The Congo (Zaire) River is the second longest (4,700 km in length) river in Africa, next to Nile. A Landsat 8 image collected on March 2, 2015 by NASA shows a distinct northerly deflection of sediment plume at the river mouth (Fig. 12). This setting is highly influenced by tidal currents (Shanmugam, 2003). In a numerical modeling of sediment plumes at Congo River mouth, Denamiel et al. (2013) considered tides, wind stress, surface heat flux, and ocean boundary conditions. Hopkins et al. (2013) traced Congo plumes for hundreds of

Fig. 12. Deflected plume associated with Congo (Zaire) River. West Africa. Landsat 8 image was collected on March 2, 2015 by NASA.

kilometers and attributed plumes' deflection to winds and the Angola Current.

Yangtze River; China, East China Sea

The Yangtze River is the longest river (about 6300 km) in Asia. Satellite images show that the Yangtze River generates both hyperpycnal and deflected hypopycnal

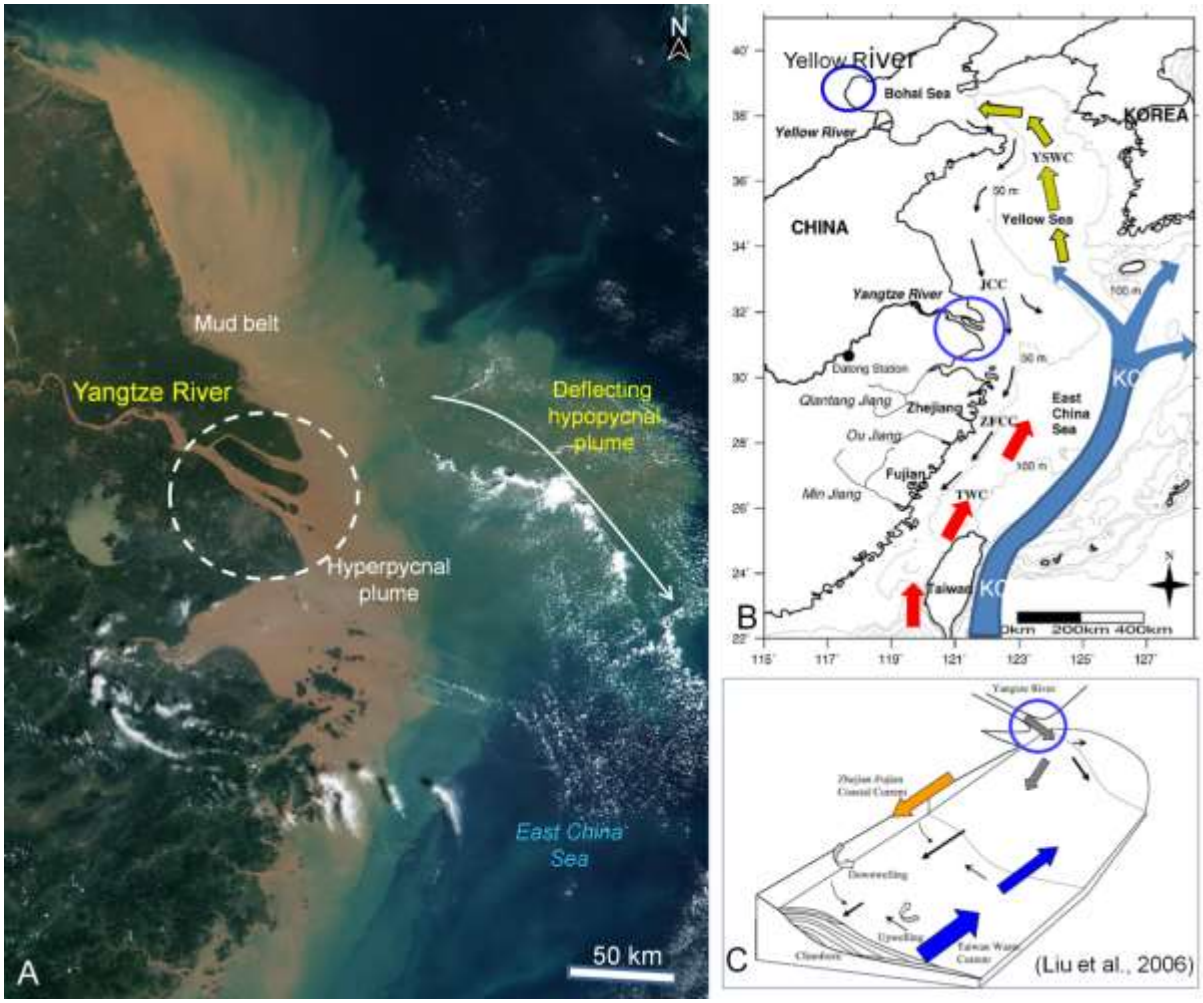

Fig. 13. Data from the Yangtze River, China. A. Satellite image showing the Yangtze River plunging into the East China Sea. Note development of both hyperpycnal plume (yellow color due to high sediment concentration) near the river mouth and hypopycnal plume (blue color due to low sediment concentration) on the seaward side. Note deflected hypopycnal flows that move southward (white arrow), possibly due to modulation by south-flowing shelf currents. In a recent study, Luo et al. (2017) recognized that extended and deflected density plumes (white arrow) tend to develop during winter months, which are absent during the summer months. Note sheet-like mud belt developed along the inner shelf due to contour-following shelf currents. White dashed circle = Yangtze River mouth. NASA. B. Map showing warm Kuroshio Current (KC) in the East China Sea and Yellow Sea. TWC = Taiwan Warm Current; YSWC = Yellow Sea Warm Current; ZFCC = Zhejiang−Fujian Coastal Current; JCC = Jiangsu Coastal Current. Blue circles: Yangtze and Yellow River mouths. From Liu et al. (2006) with additional labels by G. Shanmugam; C. Conceptual model of sedimentary and oceanographic processes affecting the sediment dispersal at both subaqueous river mouth and alongshore deposits associated with the Yangtze River. Blue circle = Yangtze River mouth.From Liu et al. (2006) with additional labels by G. Shanmuagm. Both B and C figures are used with permission from Elsevier.

plumes (Fig. 13A). The Yangtze River mouth is a complex setting in which both ocean currents and tidal currents are affecting sediment dispersal.

Unlike the Yellow River that enters a protected Bohai Bay from major ocean currents, the Yangtze River enters the East China Sea affected by the warm, north-flowing Kuroshio Current (Fig. 13B). As a consequence, muddy sediments brought by the Yangtze River are redistributed and deposited as a mud belt on the inner shelf (Wu *et al*., 2016). This mud belt is evident on the satellite images (Fig. 13A).

Yellow River, China, Bohai Bay

The Yellow River is the second longest river in China, after the Yangtze River, and at the estimated length of 5,464 km. It originates in the Bayan Har Mountains in Qinghai province of Western China, and lows through nine provinces before emptying into the Bohai Bay to the east. It is regarded as the world's largest contributor of fluvial sediment load to the ocean (Yu et al. 2011). Both lobate (Fig. 2E) and deflecting (Fig. 2F) plumes have been documented.

Wang *et al*. (2010) documented the position of the tidal front about 5 km seaward off the Yellow River mouth and explained the tide-induced density flows on the shelf (Wang et al., 2010). The importance of these numerical experiments is that the topography with a strong slope off the Yellow River mouth was a determining factor on the generation of a shear front.

The sedimentologic implication of the shear front is that it limits seaward transport of sediments (Li *et al.*, 2001; Wang *et al*., 2010). If so, the extent of sediment transport into the deep sea by hyperpycnal flows comes into question. In other words, the entire concept of hyperpycnal flows transporting sediment into the deep sea (Mulder *et al.*, 2002, 2003; Steel *et al.*, 2016; Warrick *et al*., 2013; Zavala and Arcuri, 2016) is unsupported by the Yellow River, which is considered to be a classic river for hyperpycnal flows.

Pearl River, China, South China Sea

The Pearl River system is China's third-longest river, 2,400 kilometers (1,500 mi), after the Yangtze River and the Yellow River. Satellite sea surface temperature (SST) (°C) in the northern South China Sea on 9 July 2009 (Fig. 14A) and on 24 July 2011 (Fig. 14B) show the trend of sediment plumes associated with the Pearl River. Chen et al. (2017) proposed a model for upwelling water and pathway of the Pearl

River plume in the northern South China Sea (Fig. 14C). There is clear evidence for deflecting flume and that the current direction is parallel to plume direction. Satellite images show that there was a belt of turbid water appearing along an upwelling front near the Chinese coast of Guangdong, a strong jet exists at the upwelling front with a speed as high as 0.8 m s^{-1}, which acts as a pathway for transporting the high-turbidity plume water. The dynamical analysis of Chen et al. (2017) suggests that geostrophic equilibrium dominates in the upwelling front and plume areas, and the baroclinicity of the

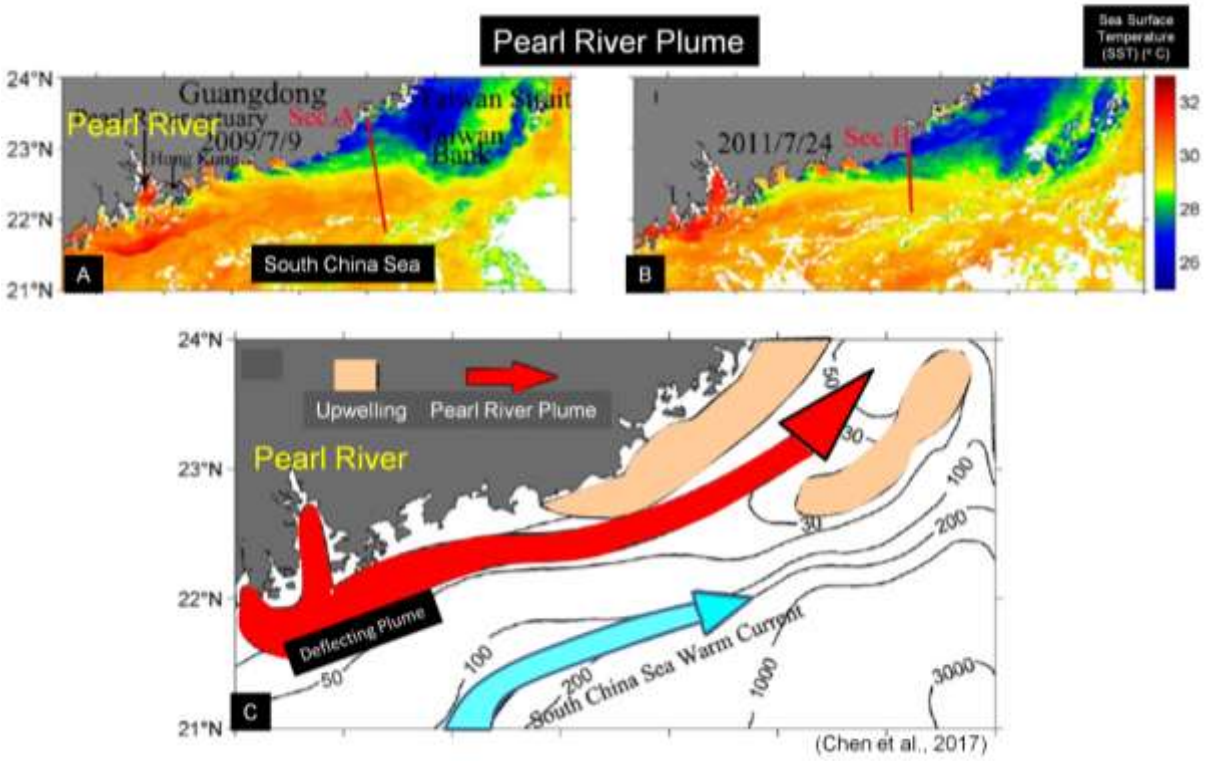

Fig. 14. Data from the Pearl River, China. Satellite sea surface temperature (SST) (°C) in the northern South China Sea on 9 July 2009 (A) and on 24 July 2011 (B) showing the Pearl River mouth and associated plumes. C. Schematics of upwelling water and pathway of the Pearl River plume in the northern South China Sea. Note that the deflecting flume (red arrow) direction is parallel to the South China Sea Warm Current (blue arrow) direction. Compiled from Chen et al. (2017) with additional color labels by G. Shanmugam. Contours show the bathymetry in meters.

and indicate that the turbid water of the Pearl River plume water could be transported to a far-reaching area east of the Taiwan Bank. Numerical modeling results are consistent with the satellite observations, and reveal that upwelling front resulting from the horizontal density gradient is responsible for the generation of the strong jet, which enhances the far-reaching transport of the terrigenous nutrient- rich water of the Pearl River plume.

Model sensitivity analyses also confirm that this jet persists as long as the upwelling front exists, even when the wind subsides and becomes insignificant.

Krishna-Godavari Rivers, India, Bay of Bengal

Both Krishna and Godavari Rivers originate in the Western Ghats and flow across the Deccan Plateau and empty their sediments into the Bay of Bengal. Well-developed deflecting plumes are evident in NASA images of the Godavari River mouth (Fig. 15). The KG Basin is a tide-influenced setting (Shanmugam et al., (2009). In this setting, monsoonal currents play an important role in southerly deflection of sediment plume (Fig. 15B).

Sridhar et al. (2008) studied the influence of seasonal geostrophic currents on sediment plumes in the Krishna-Godavari Basin. Based on the data from Indian remote sensing satellite, Oceansat-1, carries ocean color monitor [OCM] sensor, Sridhar et al. (2008) documented the suspended sediment concentrations [SSC] during 1999-2006 and illustrated a unique plume off Krishna-

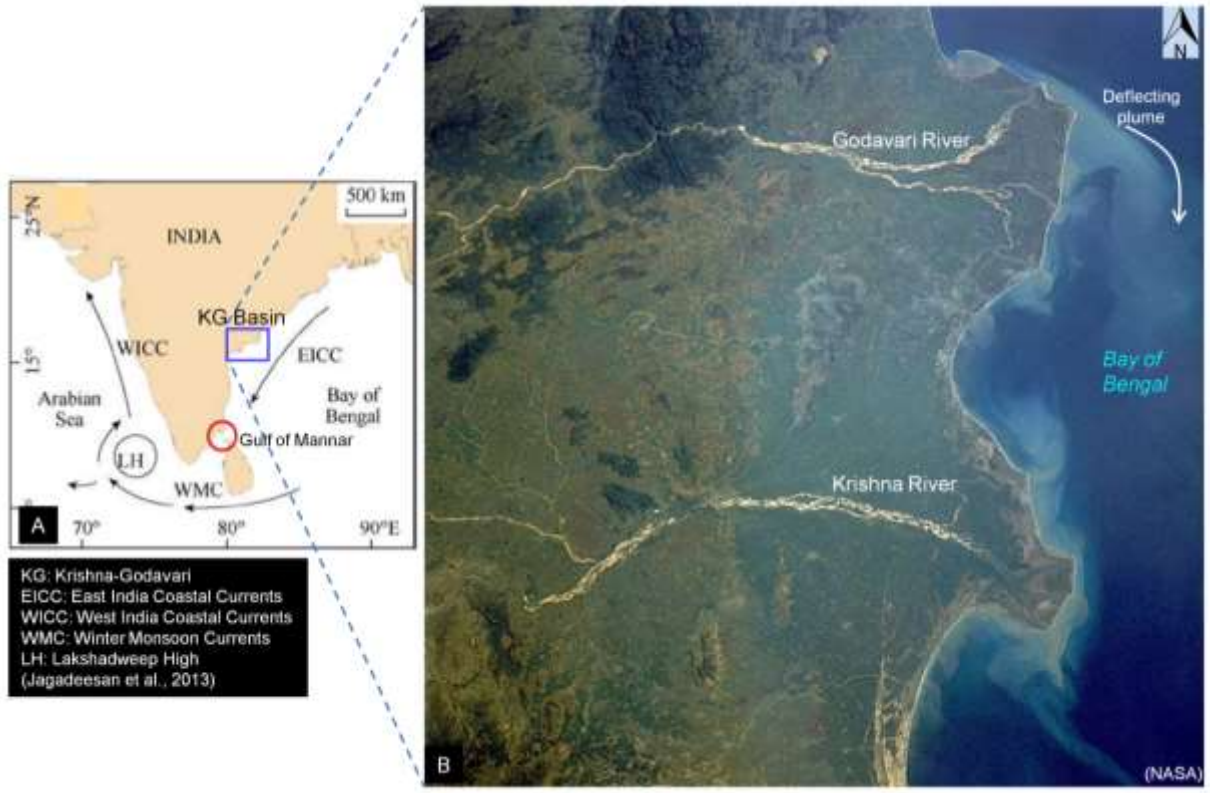

Fig. 15. Data from the Krishna-Godavari Rivers, India. A. Index map of India showing location of the Krishna-Godavari (KG) Basin and northeast monsoonal currents. Modified after Jagadeesan et al. (2013). B. image showing southerly deflecting plume at the mouth of the Godavari River. Image credit: NASA.

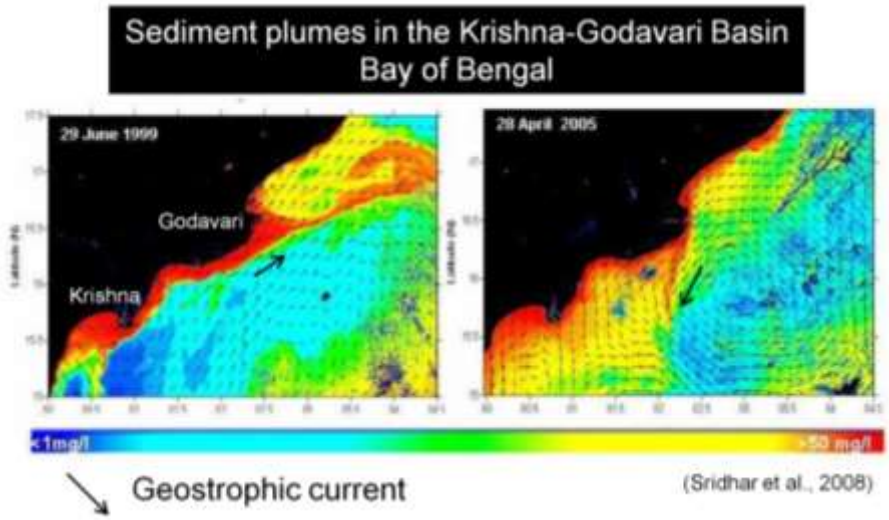

Fig. 16. Sediment plumes and geostrophic currents in the Krishna-Godavari Basin. From Sridhar et al. (2008) with additional labels by G. Shanmugam

Godavari river Basin (Fig. 16). Though high sediment concentration is present all along the east coast of India, the offshoot of the plume is present only at Krishna-Godavari Basin. The presence, extent, orientation and intensity of this plume have both seasonal and inter annual variations. Sridhar et al. (2008) superimposed the geostrophic currents over the OCM observations and documented a convincing influence of geostrophic currents on the deflection of sediment plumes (Fig. 16).

Brisbane River, Australia, Moreton Bay

The Brisbane River is located on the east coast of Australia (Fig. 17A). A storm on May 1, 2015, dropped more than 360 millimeters (14 inches) of rain within about three hours in southeast Queensland. As a result of the rainfall, flash flooding caused distinct river plumes to form along the coastline. On May 3, after the storm had passed, the Operational Land Imager (OLI) on Landsat 8 of NASA acquired a good view of a deflected plume from the Brisbane River entering Moreton Bay (Fig. 17B). In this case, the deflection was caused by the anthropogenic structure of the Port of Brisbane (Fig. 17B).

Fig. 17. Data from the Brisbane River, Australia A. Index map of Australia showing location of city of Brisbane. B. Satellite image showing deflection of the Brisbane River Plume. Note the location of Port o Brisbane and its influence on the plume direction. NASA.

Dart River, South Island, New Zealand, Lake Wakatipu

Fig. 18. Data from the Dart River, New Zealand. A. Index map showing New Zealand and position of Dart braid delta in the South Island of New Zealand. B. Aerial photograph showing Southern Alps and related fluvial setting. Note steep gradient that is typical of braid deltas (McPherson et al., 1987). C. Aerial photograph taken from a helicopter showing a well-developed braid delta with deflecting density plumes (i.e., hyperpycnal plumes) at the mouths of the Dart and Rees Rivers flowing into Lake Wakatipu at Glenorchy near Queenstown, South Island, New Zealand. The Dart River originates from the Dart Glacier in the heart of the Southern Alps to the north (i.e., left of image). Approximate width of braid delta in the image is 1.5 km. Photo by John G. McPherson, Melbourne, Australia

The Dart River originates from the Dart Glacier in the heart of the Southern Alps in the South Island of New Zealand (Fig. 18A). A photograph taken from a helicopter showing a well-developed braid delta with linear density plumes (i.e., hyperpycnal plumes) at the mouths of the Dart and Rees Rivers flowing into Lake Wakatipu at Glenorchy near Queenstown, South Island, New Zealand (Fig. 18C). High gradients of this setting (Fig. 18B) are typical of coarse-grained braid deltas (McPherson et al., 1987). The cause of plume deflection is unclear, although the area is subjected to tidal influence (Heath, 1975).

Global significance of wind forcing on sediment plumes

A review of sediment plumes suggests that there are 22 external controls (Fig. 19). Although there are 22 external factors, wind forcing is the most significant worldwide (Table 1). Wind forcing refers to wind tress exerted by the wind on bodies of water. Wind forcing is the umbrella term for various wind-related phenomena, such as wind waves, longshore currents, cyclonic currents, monsoonal currents, upwelling currents, and seiche. Milliff et al. (2004, their Fig. 5) discussed aspects of wind stress curl and wind stress divergence in illustrating the storm tracks of the Northern Hemisphere (e.g., 35° –50°N, emanating from western boundaries in both ocean basins), storm tracks in the Southern Hemisphere [e.g., 35°–50°S, the intertropical convergence zone in the eastern tropical Pacific (0° –10 °N)], and tropical cyclone regions of the Indian and western Pacific Oceans. Although tropical cyclones occur worldwide, they tend to concentrate on certain key locations, namely the Gulf of Mexico and the Bay of Bengal

Environment	Composition	Provenance	External Control	Type
1. Marine	1. Siliciclastic	1. River flood	1. Wind forcing	1. Simple lobe
2. Lacustrine	2. Calciclastic	2. Common delta	2. Wind waves	2. Horse's tail
3. Estuarine	3. Volcaniclastic	3. Braid delta	3. Longshore curr.	3. Deflecting
4. Lagoon	4. Planktonic	4.Tidal estuary	4. Cyclonic curr.	4. Dissipating
5. Bay	5. Hydrogen sulfide	5. Subglacial	5. Monsoonal curr.	5. U-Turn
6. Reef	6. Gas hydrate	6. Eolian	6. Upwelling curr.	6. Swirly
		7. Volcanic	7. Seiche	7. Cloudy
		8. Planktonic	8. Tidal shear front	8. Massive
		9. Carbonate platform/Reef	9. Tidal current	9.Tidal lobe
		10. Hydrogen sulfide	10. Internal waves and tides	10. Cascading
		11. Gas hydrate	11. Ocean curr.	11. Backwash
			12. Tsunami	12. Meltwater
			13. Braid delta	13. Coalescing irreg.
			14. Volcanism	14. Blanketing
			15. Glacial melt	15. Linear
			16. Coral reef	16. Anastomosing
			17. Fish activity	17. Coalescing lobe
			18. Pockmarks	18. Whitings
			19. Phytoplankton	19. Ring
			20. Hydrogen sulfide	20. Tendril
			21. Gas hydrate	21. Eolian dust
			22. Anthropogenic	22. Feathery
				23. Volcanic ash
				24. Gas hydrate

Fig. 19. Summary diagram showing 22 external controls. Updated after Shanmugam (2018a, b).

Shanmugam (2012) based on data from

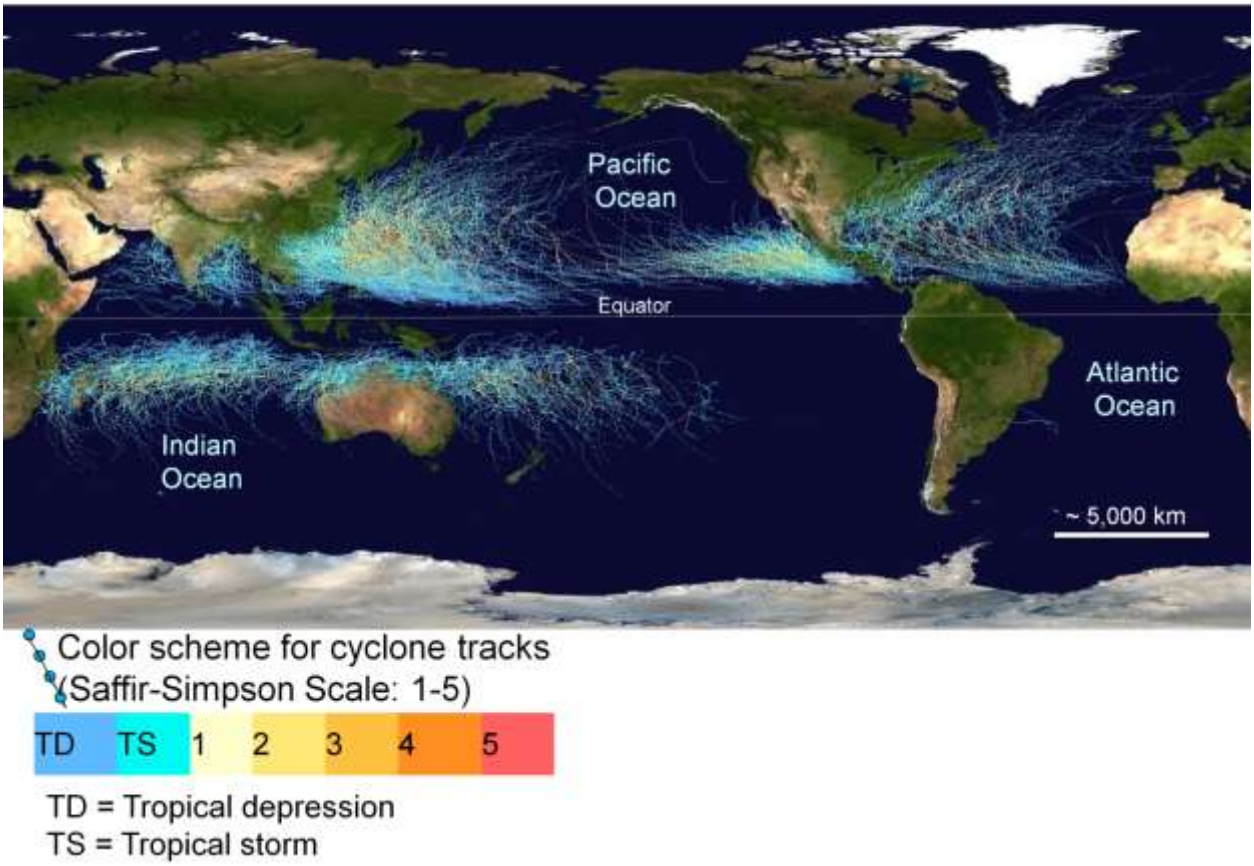

(Fig. 20). In the context of this article, the Hurricane Floyd generated 100-km wide sediment plumes on the U.S. Atlantic Margin (Fig. 21).

Fig. 20. Map showing the tracks of all tropical cyclones, which formed worldwide during the period 1985-2005. The points show the locations of the cyclones at six-hourly intervals. The color scheme represents tropical depression, tropical storm, and the Saffir-Simpson Hurricane Scale of 1-5. Note high concentration of cyclones in the Gulf of Mexico and Bay of Bengal. From NASA.

The Saffir-Simpson Hurricane Scale:

_ Category 1: 120-153 km h^{-1}

_ Category 2: 154-177 km h^{-1}

_ Category 3: 178-209 km h^{-1}

_ Category 4: 210-249 km h^{-1}

_ Category 5: >249 km h^{-1}

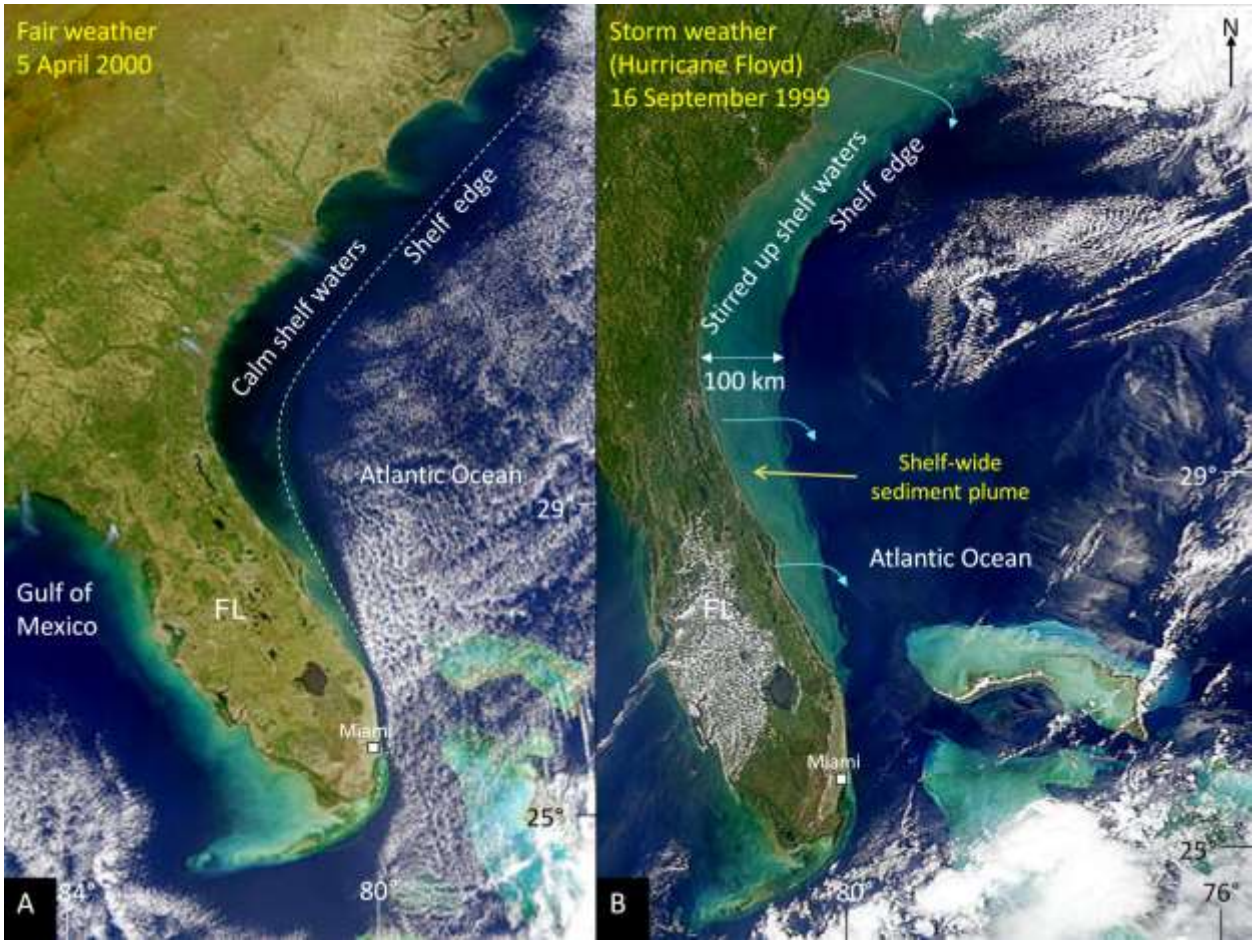

Fig. 21. Shelf-wide sediment plumes generated by Hurricane Floyd of 1999 on the U.S. Atlantic margin. (A) Satellite image showing calm shelf waters (dark blue) on a fair-weather day (April 5, 2000) along the Florida-Georgia-South Carolina-North Carolina coast. Note the influx of suspended sediments and organic matter (yellowish brown) from four rivers into the Atlantic Ocean along the coast. Dashed line indicates approximate position of the shelf edge. (B) Satellite image showing shelf-wide sediment plume (cyan color) as Hurricane Floyd (storm weather) passed over these waters on September 16, 1999. Note that the turbid zone (i.e., sediment plume) is occupying the entire shelf width, which is approximately 100 km (62 mi). Three bent arrows show trends of sediment transport into the deep Atlantic Ocean. FL = Florida. After Shanmugam (2008), reprinted by permission of the American Association of Petroleum Geologists whose permission is required for further use.

An understanding of wind forcing is critical on deflecting sediment plumes in the world's oceans at various depths. This issue can be demonstrated using empirical data from the Gulf of Mexico, which is an ideal location to study wind forcing. For example, the Loop Current in the Gulf of Mexico is a wind-driven current system (Mullins et al., 1980). Velocities in eddies that have detached from the Loop Current have been recorded as high as 200 cm s^{-1} at a depth of 100 m (Cooper et al., 1990). The Loop Current and related eddies pose significant problems for deepwater drilling (Koch et al.,

1991). For example, drilling operations in the Green Canyon 166 area were temporarily suspended in August of 1989 because of high-current velocities that reached nearly 150 cm s^{-1} at a depth of 45 m, and 50 cm s^{-1} at a depth of 250 m. These intense bottom currents affect the ability of a drilling rig to hold station over a wellhead (Koch et al., 1991). Current-velocity measurements, bottom photographs, high-resolution seismic records, and GLORIA side-scan sonar records indicate that the Loop Current influences the seafloor at least periodically in the Gulf of Mexico (Pequegnat, 1972). Computed flow velocities of the Loop Current vary from nearly 100 cm s^{-1} at the sea surface to more than 25 s^{-1} at 500 m water depth (Nowlin and Hubert, 1972). This high surface velocity suggests a wind-driven origin for these currents. Flow velocities measured using a current meter reach up to 19 cm s^{-1} at a depth of 3,286 m (Pequegnat, 1972). Kenyon et al. (2002) reported 25 cm s^{-1} current velocity measured 25 m above the seafloor. Such currents are capable of reworking fine-grained sand on the seafloor. Current ripples, composed of sand at a depth of 3,091 m on the seafloor (Pequegnat, 1972), are the clear evidence of deep bottom-current activity in the Gulf of Mexico today (Pequegnat, 1972). Therefore, wind forcing is a powerful agent in deflecting sediment plumes at various depths varying from 10s of meters to 1000s of meters.

Implications for sediment transport

A summary diagram illustrates the differences between two depositional systems, namely the normal sediment transport versus the deflected sediment transport (Fig. 22). In the normal mode, the following conventional concepts are applicable:

- Normal downslope transport from source to sink is common.
- Paleocurrent directions are reliable.
- Depositional settings cover shelf, slope, and basin.
- Wind forcing and tidal currents are common in shelf environment.
- Mass transport and bottom currents are common in slope and basin.
- There is a general increase in grain size from sink to source.
- There is a reliable compositional trend from sink to source.
- There is a reliable inference to provenance.
- At river mouths, lobate plumes (deltas, Fig. 2E) develop with predictable sand distribution. In

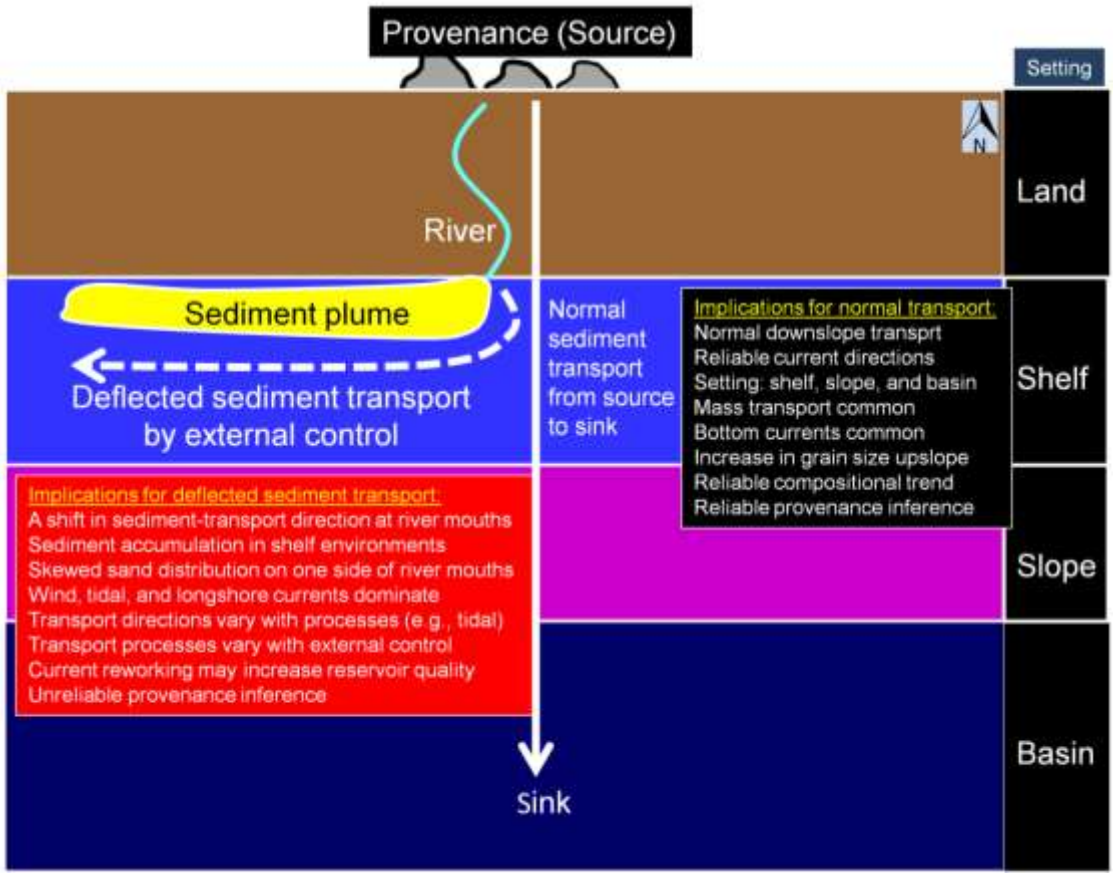

Fig. 22. Summary diagram showing the difference in sediment transport between normal mode and deflected mode with corresponding implications for paleocurrents and provenance. Compare with case study of the Elwha plume in the Strait of Juan de Fuca (Fig. 3C).

basinal environments, submarine fans tend to develop at canyon mouths with predictable sand distribution.

In the deflected mode, conventional concepts do not apply. For example (Fig. 22):

- A major shift occurs in sediment-transport direction occurs at river mouths.
- Sediment accumulation tends to occur in shelf environments, close to the shoreline.
- Sand distribution occurs on only one side of the river mouth.
- Wind, tidal, and longshore currents are dominant.
- Sediment-transport directions could vary with processes (e.g., bidirectional tidal currents).
- Transport processes may vary with external control, such as cyclones, upwelling, etc.

- Current reworking is common and therefore, traction structures are also common in sediment.
- Current reworking may increase reservoir quality.
- Because current directions are complex, it is unreliable to infer provenance accurately.
- Unlike normal sediment transport systems, sand distribution is quite different in deflected systems. For example, deflected sediment may develop tongue-like geometry (Fig. 3C), whereas normal mode develops lobate geometry at river mouths (Fig. 2E). Such a difference is important in petroleum exploration. In the case of the deflected mode, the sand abruptly ends at river mouths, and there is a total absence of sand on the western side of the river mouth in the Elwha River (Fig. 3C).

Provenance

Aspects of sediment provenance have been documented in thematic edited volumes (e.g., Zuffa, 1985; Mazumder, 2016). Principal data used in provenance studies are 1) paleocurrent directions, 2) grain size, 3) sediment composition, 4) diagenetic alteration, 5) stratigraphic framework, 6) depositional setting, and 7) tectonic deformation. Commonly, primary sedimentary structures and related current directions are used in deciphering sediment provenance (Pettijohn, 1975; Potter and Pettijohn, 1977; Zuffa, 1985; Ramos-Vázquez and Armstrong-Altrin, 2019). However, complex current directions associated with deep-water bottom currents pose immense challenges in inferring the primary sediment source (Shanmugam, 2016). This challenge is equally acute in shelf environments where sediment transport is diverted from the normal downslope mode due to external factors, such as wind forcing (Fig. 3C).

Concluding remarks

Empirical data based on satellite images and aerial photographs show that over 50% of the cases studied (i.e., 18 out of 29 cases) have been subjected to varying degrees of deflection of sediment transport, away from the normal course in a downslope direction, by external controls. These external controls include a plethora of oceanographic (e.g., ocean currents, upwelling, etc.), meteorological (e.g., wind forcing, cyclone, etc.), and gravitational (e.g., tides and tidal currents) phenomena. In

particular, wind forcing is the most dominant external control of sediment plumes on the shelf and slope environments. The importance of these findings is that our failure to establish external controls on sediment plumes in the ancient sedimentary record could result in erroneous depositional models in terms of sediment transport, paleogeography, and provenance with implications for predicting unrealistic sand distribution and reservoir quality in petroleum exploration of both shallow- and deep-water settings.

Acknowledgements

I thank Prof. G. N. Nayak, CSIR Emeritus Scientist at School of Earth, Ocean and Atmospheric Sciences, Goa University, Goa, India, who is also the President of the Indian Association of Sedimentologists, for a thorough and helpful review of this paper. I also than the second reviewer Dr. Mayla Ramos-Vazquez for helpful review. I am grateful to Dr. John S. Armstrong-Altrin, National Autonomous University of Mexico, for handling my paper. I thank both Managing Editors of the journal, Prof. G. M. Bhat and Dr. Bashir Ahmad Lone, both of Jammu University, India, for their help with editorial matters. I am grateful to NASA (National Aeronautics and Space Administration) for their excellent collection of satellite and other images of density plumes triggered by river floods. I thank Mr. Tom Roorda, Port Angeles, Washington, USA, for giving permission to use aerial photograph of a spectacular sediment plume that was triggered by the demolition of Elwha Dam in 2012 (Fig. 3C) and the Elwha River mouth without sediment plume in 2019 (Fig. 3D). Tom Roorda also provided Meta Data for Elwha plume photographs. I also thank Dr. John G. McPherson, Melbourne, Australia, for proving aerial photographs taken from a helicopter of Dart River braid delta in New Zealand. As always, I am thankful to my wife Jean Shanmugam for her general comments.

References

Arnau, P., Liquete, C. and Canals, M. (2004). River mouth plume events and their dispersal in the northwestern Mediterranean Sea. Oceanography, 17 (3), 23–31

Balasubramanian, T., and Ajmal Khan, S. (2002). Estuaries of India. Environmental information system Centre, Centre of Advanced Study in marine biology, Annamalai University, Parangipettai-608 502, Tamil Nadu, India, sponsored by the Ministry of Environment & forests, government of India, 195. New Delhi: ENVIS Publication Series: 1/2002.

Bates, C.C., (1953). Rational theory of delta formation. AAPG Bulletin, 37, 2119-2162.

Beckers, A., Beck, C., Hubert-Ferrari, A., Tripsanas, E., Crouzet, C., Sakellariou, D., Papatheodorou. G., de Batist, M. (2016). Influence of bottom currents on the sedimentary processes at the western tip of the Gulf of Corinth, Greece. Marine Geology, 378, 312-332.

Brink, K.H. (2016}. Cross-shelf exchange. Annual Review of Marine Science, 8, 59-78.

Cannon, G. A. (1978). Circulation In the Strait of Juan De Fuca: Some Recent Oceanographic Observations. NOAA Technical Report ERL 399-PMEL 29, 55 p.

Chen, Z., Pan, J. Jiang, Y. and Lin, H. (2017). Far-reaching transport of Pearl River plume water by upwelling jet in the northeastern South China Sea. Journal of Marine Systems, 173, 60-69

Cooper, C., Forristall, G.Z., and Joyce, T.M., (1990). Velocity and hydrographic structure of two Gulf of Mexico warm-core rings. Journal of Geophysical Research, 95 (C2), 1663-1679.

Cutroneo, L., Ferretti, G., Scafidi, D., Ardizzone, G. D., Vagge, G., and Capello, M., (2017). Current observations from a looking down vertical V-ADCP: interaction with winds and tide? The case of Giglio Island (Tyrrhenian Sea, Italy). Oceanologia, 59 (2), 139-152.

Denamiel, C., Budgell, W. P., and Toumi, R. (2013). The Congo River plume: Impact of the forcing on the far-field and near-field dynamics, Journal of Geophysical Research: Oceans, 118, 964–989, doi:10.1002/jgrc.20062

Duda, J.J., Warrick, J.A., and Magirl, C.S., (2011). Coastal and Lower Elwha River, Washington, Prior to Dam Removal—History, Status, and Defining Characteristics. In: Duda, J.J., Warrick, J.A., Magirl, C.S., (Eds.), Coastal Habitats

of the Elwha River: Biological and Physical Patterns and Processes Prior to Dam Removal. U.S. Geological Sand Survey Scientific Investigations Report 2011-5120. Chapter 1.

Foreman, M. G. G., Callendar, W., MacFadyen, A., Hickey, B. M., Thomson, R. E., and di Lorenzo, E., (2008). Modeling the generation of the Juan de Fuca Eddy. Journal of Geophysical Research: Oceans, 113, C3, CiteID C03006

Fossati, M. Cayocca, F., and Piedra-Cueva. I. (2014). Fine sediment dynamics in the Río de la Plata. Advances in Geosciences, 39, 75–80.

Fossati, M., and Piedra-Cueva. I. (2013). A 3D hydrodynamic numerical model of the Río de la Plata and Montevideos coastal zone. Applied Mathematical Modelling, 37, 1310–1332.

Framiñan, M.B., and Brown. O.B. (1996). Study of the Río de la Plata turbidity front, part I: spatial and temporal distribution. Continental Shelf Research, 16, 1259–1282.

Geyer, W. R., Hill, P., Milligan, T.G., and Traykovski, P. A. (2000). The structure of the Eel River plume during flood. Continental Shelf Research, 20(16), 2067-2093

Gonzalez-Silvera, A., Santamaria-del-Angel, E., and Millán-Núñez, R. (2006). Spatial and temporal variability of the Brazil–Malvinas Confluence and the La Plata Plume as seen by SeaWiFS and AVHRR imagery. Journal of Geophysical Research, 111, C06010.

Heath, R. A. (1975) Surface oscillations of lake Wakatipu, New Zealand, New Zealand Journal of Marine and Freshwater Research, 9:2, 223-238, DOI: 10.1080/00288330.1975.9515560

Hickey, H., (2013). Tracking sediments' fate in largest-ever dam removal. UW News (U. Washington), Seattle, WA, March 7, 2013. With technical information on sediment plumes from two UW oceanographers: Charles Nittrouer and Andrea Ogston. <http://www.washington.edu/news/2013/03/07/tracking-sediments-fate-in-largest-ever-dam-removal/> Accessed March 3, 2019

Hopkins, J., Lucas, M., Dufau, C., Sutton, M., and Lauret, O., (2013). Detection and variability of the Congo River plume from satellite derived sea surface temperature, salinity, ocean colour and sea level. EGU General Assembly 2013, held 7-12 April, 2013 in Vienna, Austria, id. EGU2013-3135

Imran, J., and J. Syvitski. (2000). Impact of extreme river events on coastal oceans. Oceanography, 13 (3), 85–92.

Jagadeesan, L., Jyothibabu, R., Anjusha, A., Mohan, A.P., Madhu, N.V., Muraleedharan, K.R., and Sudheesh, K., (2013). Ocean currents structuring the mesozooplankton in the Gulf of Mannar and the Palk Bay, southeast coast of India. Progress in oceanography, *110*, 27-48.

Kenyon, N.H., Akhmetzhanov, A.M., and Twichell, D.C., 2002. Sand wave fields beneath the Loop Current, Gulf of Mexico: reworking of fan sands. Marine Geology, 192, 297-307.

Klein, G. D. (1970). Depositional and dispersal dynamics of intertidal sand bars. Jour. Sedimentary Petrology, 40, 1095-1127.

Koch, S.P., Barker, J.W., Vermersch, J.A., 1991. The Gulf of Mexico Loop Current and deepwater drilling. Journal of Petroleum Technology, 43, 1046-1050 and 1118-1119.

Komar, P. D., 1976, Beach processes and sedimentation: Englewood Cliffs, New Jersey, Prentice-Hall, Inc., 429 p.

Li, G.X., Tang, Z.S., Yue, S.H., Zhuang, K.L., and Wei, H.L., (2001). Sedimentation in the shear front off the Yellow River mouth. *Continental Shelf Research*, 21 (6–7), 607–625.

Liu, J.P., Li, A.C. Xu, K.H. Velozzi, D.M. Yang, Z.S. Milliman, J.D. and DeMaster. D.J. (2006). Sedimentary features of the Yangtze River-derived along-shelf clinoform deposit in the East China Sea. Continental Shelf Research, 26, 2141–2156.

Luo, Z., Zhu, J. Wu, H. and Li. X. (2017). Dynamics of the sediment plume over the Yangtze Bank in the Yellow and East China Seas. Journal of Geophysical Research: Oceans 122: 10,073–10,090 https://doi.org/10.1002/2017JC013215.

Manca, F., Capelli, G., La Vigna, F., Mazza, R., and Pascarella, A., (2014). Wind-induced salt-wedge intrusion in the Tiber River mouth (Rome-Central Italy). Environmental Earth Sciences, 72 (4), 1083-1095

Matano, R.P., Palma, E.D. and Piola. A.R. (2010). The influence of the Brazil and Malvinas Currents on the southwestern Atlantic shelf circulation. Ocean Science, 6, 983–995.

Mazumder, R. (Ed.), (2016). Sediment Provenance: Influences on Compositional Change from Source to Sink. Elsevier, 614 p.

McPherson, J.G., Shanmugam, G. and Moiola. R.J. (1987). Fan-deltas and braid deltas: Varieties of coarse-grained deltas. GSA Bulletin, 99, 331–340.

Middleton, G.V., and Hampton, M.A., 1973. Sediment gravity flows: mechanics of flow and deposition. In: Middleton, G.V., Bouma, A.H. (Eds.), Turbidites and Deep-Water Sedimentation. SEPM, Anaheim, CA, pp. 1-38. SEPM Pacific section Short Course.

Mikhailova, M. V., Bellotti, P., Valeri, P., and Tortora, P., (1998). The Tiber River Delta and the Hydrological and Morphological Features of Its Formation. Water Resources. Vol. 25, Mo. 5, 572-582. Translated from Vodnye Resursy, 25 (5), 620-630.

Mikhailov, V.N., Kravtsova, V.I. and Isupova. M.V. (2015). Impact of reservoirs on the hydrological regime and morphology of the lower reaches and delta of the Zambezi River (Mozambique). Water Resources, 42 (2), 170–185.

Milli, S., et al. (2013). The transition from wave-dominated estuary to wave-dominated delta: The Late Quaternary stratigraphic architecture of Tiber River deltaic succession (Italy). Sedimentary Geology, 284, 159-180.

Milliff, R. F., Morzel, J., Chelton, D. B., and Freilich, M. H., (2004). Wind Stress Curl and Wind Stress Divergence Biases from Rain Effects on QSCAT Surface Wind Retrievals. Journal of Atmospheric and Oceanic Technology, 21, 8, 1216-1231.

Mulder, T., Migeon, S., Savoye, B. and Faugères, J.-C. (2002). Reply to discussion by Shanmugam on Mulder et al. (2001, Geo-Marine Letters, 21, 86–93) Inversely graded turbidite sequences in the deep Mediterranean. A record of deposits from flood-generated turbidity currents? Geo-Marine Letters, 22, 112–120.

Mulder, T., Syvitski, J.M., Migeon, S., Faugeres, J.-C., and Savoye, B., (2003). Marine hyperpycnal flows: initiation, behavior and related deposits: a review. Marine and Petroleum Geology, 20, 861-882.

Mullins, H.T., Neumann, A.C., Wilber, R.J., Hine, A.C., and Chinburg, S.J., 1980. Carbonate sediment drifts in the northern Straits of Florida. AAPG Bulletin, 64, 1701-1717.

NASA (National Aeronautics and Space Administration), (2019). Earth Observatory. <https://earthobservatory.nasa.gov/.> Accessed January 30, 2018.

NOAA (National Oceanic and Atmospheric Administration) Fisheries Glossary, (2006). River plume. NOAA Technical Memorandum NMFS-F/SPO-69. Revised Edition, U.S. Department of Commerce, 71 p.

Nowlin Jr., W.D., and Hubert, J.M., 1972. Contrasting summer circulation patterns for the eastern Gulf. In: Capurro, L.R.A., Reid, J.L. (Eds.), Contributions on the Physical Oceanography of the Gulf of Mexico, Texas A&M University Oceanographic Studies 2. Gulf Publishing, Houston, TX, pp. 119-137.

Peliz, A., Marchchesiello, P., Santos, A.M.P., Dubert, J., A. Teles-Machado, A. and Marta-Almeida. M. (2009). Surface circulation in the Gulf of Cadiz: 2. Inflowoutflow coupling and the Gulf of Cadiz slope current. Journal of Geophysical Research: Oceans, 114, C03011.

Pequegnat, W.E., (1972). A deep bottom-current on the Mississippi Cone. In: Capurro, L.R.A., Reid, J.L. (Eds.), Contribution on the Physical Oceanography of the Gulf of Mexico, Texas A&M University Oceanographic Studies 2. Gulf Publishing, Houston, TX, pp. 65-87.

Pettijohn, F.J., (1975). Sedimentary Rocks, third ed. Harper & Row, Publishers, New York, 628 p.

Potter, P.E., and Pettijohn, F.J., (1977). Paleocurrents and Basin Analysis. Springer, 425 p.

Ramos-Vázquez, M.A., Armstrong-Altrin, J.S. (2019). Sediment chemistry and detrital zircon record in the Bosque and Paseo del Mar coastal areas from the southwestern Gulf of Mexico. Marine and Petroleum Geology, 110, 650-675.

Ritchie, A.C., Warrick, J.A., East, A., et al. (2018). Morphodynamic evolution following sediment release from the world's largest dam removal. Scientific Reports | *(2018) 8:13279* + DOI:10.1038/s41598-018-30817-8 1, 13 p.

Shanmugam, G. (2003). Deep-marine tidal bottom currents and their reworked sands in modern and ancient submarine canyons. Marine and Petroleum Geology, 20, 471–491

Shanmugam, G., (2008).The constructive functions of tropical cyclones and tsunamis on deepwater sand deposition during sea level highstand: implications for petroleum exploration. *AAPG Bulletin*, 92, 443-471

Shanmugam, G., (2012). New Perspectives on Deep-water Sandstones, Origin, Recognition, Initiation, and Reservoir Quality. Handbook of Petroleum Exploration and Production, vol. 9. Elsevier, Amsterdam, 524 p.

Shanmugam, G., (2016). The contourite problem. In: Mazumder, R. (Ed.), Sediment Provenance. Elsevier, pp. 183–254.

Shanmugam, G. (2018a). The hyperpycnite problem. Journal of Palaeogeography, 7 (3), 197-238.

Shanmugam, G.. (2018b). A global satellite survey of density plumes at river mouths and at other environments: Plume configurations, external controls, and implications for deep-water sedimentation. Petroleum Exploration and development, 45 (4), 640-661.

Shanmugam, G., Shrivastava, S. K., and Das, B. (2009). Sandy debrites and tidalites of Pliocene reservoir sands in upper-slopecanyon environments, offshore Krishna- Godavari Basin (India), implications. Journal of Sedimentary Research, 79, 736-756.

Southard, J.B., and Stanley, D.J., (1976}. Shelf-break processes and sedimentation. In: Stanley, D.J., Swift, J.P. (Eds.), Marine Sediment Transport and Environmental Management. John Wiley & Sons, New York, pp. 351-377.

Sridhar, P. N., Ali, M. M., Vethamony, P., Babu, M. T., Ramana, V., and Jayakumar, S. (2008). Seasonal occurrence of unique sediment plume in the Bay of Bengal. Eos Transactions American Geophysical Union, 89(3), 22-23.

Steel, E., Simms, A.R., Warrick, J., and Yokoyama, Y., (2016). Highstand shelf fans: The role of buoyancy reversal in the deposition of a new type of shelf sand body. *GSA Bulletin*, 128, 1717–1724.

Thomson, R. E., MihálLy, S. F.,and Kulikov, E. A ., (2007). Estuarine versus transient flow regimes in Juan de Fuca Strait. Journal of Geophysical Research: Oceans, 112, C9, CiteID C09022

USGS (U.S. Geological Survey) (2018). Moving Mountains: Elwha River Still Changing Five Years After World's Largest Dam-Removal Project: More than 20 million tons of sediment flushed to the sea. USGS News. September 5, 2018.

<https://www.usgs.gov/news/moving-mountains-elwha-river-still-changing-five-years-after-world-s-largest-dam-removal> Accessed March 3, 2019.

Walker, N.D. and Rouse, Jr. L.J. (1993). Satellite assessment of Mississippi River discharge plume variability. OCS Study MMS 93–0044. U.S. Dept. of the Interior, Minerals Management Service, Gulf of Mexico OCS Regional Office, New Orleans, La. 50 p.

Wang, H., Bi, N. Wang, Y. Saito, Y. and Yang. Z. (2010). Tide-modulated hyperpycnal flows off the Huanghe (Yellow River) Mouth, China. Earth Surface Processes and Landforms, 35 (11), 1315–1329.

Warrick, J. A., Stevens, A. W. Miller, J. M., and Gelfenbaum, G., (2011). Coastal Processes

of the Elwha River Delta. In: Duda, J.J., Warrick, J.A., Magirl, C.S., (Eds.), Coastal Habitats of the Elwha River: Biological and Physical Patterns and Processes Prior to Dam Removal. Chapter: 1. U.S. Geological Survey Scientific Investigations Report 2011-5120. Chapter 5.

Warrick, J.A., Simms, A.R., Ritchie, A., Steel, E., Dartnell, P., Conrad, J.E., and Finlayson, D.P., (2013). Hyperpycnal plumederived fans in the Santa Barbara Channel, California. *Geophysical Research Letters*, 40, 2081–2086.

Wu, J., Ren, J., Liu, H., Qiu, C., Cui, Y., and Zhang, Q., (2016). Trapping and escaping processes of Yangtze River-derived sediments to the East China Sea. In: Clift, P.D., Harff, J., Wu, J., Qui, Y., (Eds.), *River-Dominated Shelf Sediments of East Asian Seas*. *Geological Society, London, Special Publications*, 429, 153–169.

Yu, J., Fu, Y. Li, Y., Han, G., Wang, Y., Zhou, D., Sun, W., Gao, Y., and Meixner, F.X. 2011. Effects of water discharge and sediment load on evolution of modern Yellow River Delta, China, over the period from 1976 to 2009. Biogeosciences, 8 (9), 2427–2435.

Zavala, C. and Arcuri, M. (2016). Intrabasinal and extrabasinal turbidites: Origin and distinctive characteristics. Sedimentary Geology, 337, 36–54.

Zuffa, G.G. (Ed.), (1985). Provenance of Arenites. D. Reidel Publishing Company, Dordrecht, 408 p.